International Journal of Non-Linear Mechanics 77 (2015) 325–341

Contents lists available at ScienceDirect

International Journal of Non-Linear Mechanics

journal homepage: www.elsevier.com/locate/nlm

Lie symmetry solutions for two-phase mass flows

Sayonita Ghosh Hajra [a,*], Santosh Kandel [b], Shiva P. Pudasaini [c]

[a] Department of Mathematics, University of Utah, 155 S. 1400 E. Salt Lake City, UT 84112, USA
[b] Max Planck Institute for Mathematics, Vivatsgasse 7, 53111 Bonn, Germany
[c] University of Bonn, Steinmann Institute, Department of Geophysics, Meckenheimer Allee 176, D-53115 Bonn, Germany

ARTICLE INFO

Article history:
Received 25 June 2015
Received in revised form
10 September 2015
Accepted 10 September 2015
Available online 25 September 2015

Keywords:
Analytical solutions
Debris flow
Lie Symmetry
Mass flow
Similarity solutions
Two-phase mixture

ABSTRACT

We apply Lie symmetry method to a set of non-linear partial differential equations, which describes a two-phase rapid gravity mass flow as a mixture of solid particles and viscous fluid down a slope (Pudasaini, J. Geophys. Res. 117 (2012) F03010, 28 pp [1]). In order to systematically explore the mathematical structure and underlying physics of the two-phase mixture flow, we generate several similarity forms in general form and construct self-similar solutions. Our analysis generalizes the results, obtained by applying the Lie symmetry method to relatively simple single-phase pressure-driven gravity mass flows, to the two-phase mass flows that include several dominant driving forces and strong phase-interactions. Analytical and numerical solutions are presented for the symmetry-reduced homogeneous and non-homogeneous systems of equations. Analytical and numerical results show that the new models presented here can adequately describe the dynamics of two-phase debris flows, and produce observable phenomena that are consistent with the physics of the flow. The solutions are strongly dependent on the choice of the symmetry-reduced model, as characterized by the group parameters, and the physical parameters of the flows. These solutions reveal strong non-linear and distinct dynamic evolutions, and phase-interactions between the solid and fluid phases, namely the phase-heights and phase-velocities.

1. Introduction

Gravity mass flows and gravity currents, including avalanches, debris flows, debris floods, floods, and water waves, play important role both in environment, geophysics and engineering [2–12]. Debris flows are extremely destructive and dangerous natural hazards, so there is a need for reliable methods for predicting the dynamics, runout distances, and possible areas hit by such events. Debris flows are effectively two-phase, gravity-driven mass flows consisting of randomly dispersed interacting phases of solid grains mixed with fluid. Two-phase granular-fluid mixture flows are characterized primarily by the relative motion between the solid and fluid phases. The evolution of the solid and the fluid phases depends on the mixture composition, solid–fluid interactions, and the dynamics as modelled by the main driving forces. As observed in natural debris flows, the solid and fluid phase velocities may deviate substantially from each other, essentially affecting flow mechanics. For this reason, there has been extensive field, experimental, theoretical, and numerical investigations on the dynamics, consequences, and mitigation measures as well as industrial applications of these flows [12–16].

Significant research in the past few decades has focused on different aspects of two-phase debris avalanches and debris flows [2–10] which was recently advanced in a comprehensive theory that accounts for the different interactions between the solid particles and the fluid [1]. This model includes several fundamentally important and dominant physical aspects, including the enhanced non-Newtonian viscous stress, the virtual mass, and the generalized drag. The model constitutes the most generalized two-phase flow model to date, and can reproduce results from previous simple models that considered single- and two-phase avalanches and debris flows as special cases [1]. An important aspect of the model is the strong interactions between the solid and the fluid phases, e.g., through the hydraulic pressure gradients, buoyancy, and solid volume fraction, that control the flow dynamics. The equations are formulated as a set of well-structured partial differential equations in conservative form [1,12,17]. Here, we apply the Lie group and symmetry method to this two-phase mass flow model. We construct symmetry groups corresponding to the system of non-linear partial differential equations for the two-phase mass flows down a slope.

Lie developed the theory of Lie groups as an important tool for understanding and analyzing differential equations and to construct their solutions [18]. The Lie group of transformations leaves the underlying model equations invariant. The main idea behind applying the Lie group (Lie algebra) theory lies in constructing

* Corresponding author. Tel.: +1 8015814278.
E-mail address: Sayonita@math.utah.edu (S. Ghosh Hajra).

http://dx.doi.org/10.1016/j.ijnonlinmec.2015.09.010
0020-7462/

symmetry groups (symmetry algebras) of (partial) differential equations, obtaining the general reduced forms with fewer independent variables and finding the similarity solutions. For instance, a system of partial differential equations with two independent variables can be reduced to a system of ordinary differential equations with only one independent variable by using the Lie symmetry method. This is achieved by using the characteristic equation associated with the symmetry groups (symmetry algebras) of the underlying system. Any symmetry reduced system is characterized by a set of similarity-variables (a set of fewer new independent variables) which can be obtained by combining the original independent variables (say, time and space), and a number of similarity forms (that is less than or equal to the number of unknowns in the original system) that are invariant under the symmetry group transformations. This offers an opportunity to construct (exact) solutions in similarity forms which can be back-transformed to construct the solutions for the unknown dynamical field-variables (say, velocities and deformations).

The Lie group theory has been extensively used to obtain solutions of differential equations arising from wide range of physical problems, including the reduction of differential equations, order reduction of ordinary differential equations, construction of invariant solutions, and mapping between the solutions in mechanics, applied mathematics and mathematical physics, and applied and theoretical physics [11,19–27]. Lie algebra and symmetry group theory is an important and effective method for solving a system of non-linear partial differential equations via similarity forms and similarity solutions [19,23,27–32]. Particularly related to our interest, Lie theory has been successively applied to construct and investigate self-similar solutions to gravity currents, and relatively simple shallow water or two-layer shallow water flows, impulse modified shallow water equations, dispersive shallow-water flows, Benney system, generalized Burgers equation, etc. [11,25–27,33–37].

To our knowledge, except in [38] for which Lie symmetry method is applied for single-phase shallow frictional dry granular flows down an incline, mostly in the literature, the investigated systems are essentially single-phase, inviscid and pressure-driven shallow water flows in horizontal channels with no friction (either viscous or particle). Similarity forms for two-layer shallow water equations are derived and discussed in [27]. In their formulation, the coupling is via the reduced gravity parameter. In our two-phase mass flow model, the driving forces consist of gravity, buoyancy, and hydraulic pressure gradients for the solid and fluid phases. Further, there are strong non-linear interactions between the phases via these pressure gradients, or the pressure parameters, buoyancy, and volume fraction of solid (and fluid, because these are complimentary).

Importantly, with the Lie symmetry transformations, we show that the similarity variable for the reduced equations associated with our two-phase mass flow model takes a form of a product of two exponents in time and space, and that the similarity form (in terms of the new similarity variable) is expressed as a product of an exponent function (in time or space) and the original dynamical variables. Thus, our solutions generalize several similarity variables and similarity forms obtained in the literature by using Lie symmetry group transformations [11,25–27,33–37]. It appears that the choice of group parameters determines the similarity forms and the dynamics of the reduced system of equations. We show that, for some choices of group parameters, the reduced systems become homogeneous set of ordinary differential equations (ODEs) for which analytic similarity solutions are constructed. In general, for given sets of general group parameters, the similarity reduced forms result in different system of non-homogeneous ODEs for which similarity solutions are presented numerically.

Exact and analytical solutions to simplified cases of non-linear debris avalanche model equations are necessary to calibrate numerical simulations of flow depth and velocity profiles on inclined surfaces. These problem-specific solutions provide important insight into the full behavior of the system [10,39]. It helps better understand the basic features of the complex and non-linear governing equations. For this reason, this paper is mainly concerned about the systematic study of the phase interactions between the solid and fluid components in a two-phase mass flow. This is achieved by constructing model solutions by employing the Lie group symmetry methods. We obtain different similarity reduced forms, and present the corresponding similarity solutions. The results obtained with symmetry group properties allow us for better understanding of the complex mathematical structure and highly non-linear physical characteristics of the coupled two-phase mass flows. We present some new Lie theoretic analytical solutions to the system of partial differential equations describing the two-phase mass flows. New analytical models and results demonstrate that there are strong phase-interactions in a two-phase debris flow. Such results are not yet available in the literature. These results highlight the basic physics associated with the two-phase nature of the mixture flow, with application to a wide range of two-phase industrial and geophysical mass flows, including particle-laden and dispersive flows, sediment transport, and debris flows. Simulation results are compatible with the physics of flow.

2. The physical–mathematical model

Here, we consider the general two-phase debris flow model [1] and reduce it to one-dimensional inclined channel flow [12,17] and construct Lie group solutions for flows in an inclined channel. For simplicity, here we begin by assuming that for the solid-phase the drag force is dominated by gravity, friction and pressure-gradient, which also implies that the virtual mass force is negligible. In addition, for fluid-phase, we assume that the flow is dominated by gravity and pressure-gradient. Then, the depth-averaged mass and momentum conservation equations for the solid and fluid phases are as follows:

$$\frac{\partial h_s}{\partial t}+\frac{\partial Q_s}{\partial X}=0,\quad \frac{\partial h_f}{\partial t}+\frac{\partial Q_f}{\partial X}=0, \tag{1}$$

$$\frac{\partial Q_s}{\partial t}+\frac{\partial}{\partial X}\left(Q_s^2 h_s^{-1}\right)+\frac{\partial}{\partial X}\left(\frac{\beta_s}{2}h_s(h_s+h_f)\right)=h_s S_s,\quad \frac{\partial Q_f}{\partial t}+\frac{\partial}{\partial X}\left(Q_f^2 h_f^{-1}\right)+\frac{\partial}{\partial X}\left(\frac{\beta_f}{2}h_f(h_f+h_s)\right)=h_f S_f, \tag{2}$$

where the source terms are given by $S_s=\sin\zeta-\tan\delta(1-\gamma)\cos\zeta$ and $S_f=\sin\zeta$.

The dynamical variables and parameters are

$$h_s=\alpha_s h,\ h_f=\alpha_f h;\quad Q_s=h_s u_s=\alpha_s h u_s,\ Q_f=h_f u_f=\alpha_f h u_f;$$
$$\beta_s=\varepsilon K p_{b_s},\quad \beta_f=\varepsilon p_{b_f},\quad p_{b_f}=\cos\zeta,\quad p_{b_s}=(1-\gamma)p_{b_f},$$
$$\alpha_f=1-\alpha_s,\ \gamma=\frac{\rho_f}{\rho_s}. \tag{3}$$

In the above model equations, t is the time, X and Z are coordinates along and normal to the slope, and $\sin\zeta$ and $\cos\zeta$ are the components of gravitational acceleration with the slope inclination ζ. The solid and fluid constituents are denoted by the suffices s and f respectively. h is the mixture flow depth measured along Z, u_s and u_f are respectively the solid and the fluid velocities in the X direction. ρ_s, ρ_f, and α_s, α_f denote the densities and volume fractions of the solid particles and the fluid respectively. L and H are the typical length and depth of the flow respectively and $\varepsilon=H/L$ is the aspect ratio. K is the earth pressure coefficient. Both K and $\tan\delta$, where δ is the friction angle, include frictional behavior of

the solid-phase. p_{b_f} and p_{b_s} are associated with the effective fluid and solid pressures at the base respectively, β_s and β_f are the hydraulic pressure parameters associated with the solid- and the fluid-phases respectively, and γ is the density ratio, $(1-\gamma)$ indicates the buoyancy reduced solid normal load. $h_s=\alpha_s h$ and $h_f=\alpha_f h$ are the solid and fluid fractions in the mixture respectively, and $Q_s=h_s u_s$ and $Q_f=h_f u_f$ are the respective solid and fluid fluxes. Importantly, the system is directly and strongly coupled through the pressure gradients associated with β_s and β_f that include the cross-coupling between h_s and h_f. The model system (1) and (2) is coupled dynamically and intrinsically through the solid (or fluid) volume fraction α_s, because dynamical phase variables $Q_s, Q_f; h_s, h_f$ are defined in terms of h and α_s. Further, the phase interactions are also included via buoyancy, the terms associated with $(1-\gamma)$ in the friction and pressure parameters.

It is convenient to reduce (1) and (2) into a homogeneous system. This is achieved by the transformation

$$x=X-S_s t^2/2,\quad y=X-S_f t^2/2,\quad \hat{Q}_s=Q_s-h_s S_s t,\quad \hat{Q}_f=Q_f-h_f S_f t. \tag{4}$$

Here, x and y are associated with the moving spatial coordinates for the solid and fluid respectively, and are distinguished only by the solid and fluid net driving forces, S_s and S_f respectively. Since S_s and S_f are independent, x and y are considered as independent variables. Interestingly, for frictionless solid grains, or a neutrally buoyant solid (i.e., $\gamma=1$), the mixture behaves as an effectively single-phase bulk, and the material properties are non-distinguishable. Then, as $S_s=S_f=\sin\zeta$, in this idealized situation, $x=y$ and the complexity reduces largely. Otherwise, in general, with (4) Eqs. (1) and (2) reduce to a homogeneous system of partial differential equation:

$$\frac{\partial h_s}{\partial t}+\frac{\partial \hat{Q}_s}{\partial x}=0,\quad \frac{\partial h_f}{\partial t}+\frac{\partial \hat{Q}_f}{\partial y}=0, \tag{5}$$

$$\frac{\partial \hat{Q}_s}{\partial t}+\frac{\partial}{\partial x}\left(\hat{Q}_s^2 h_s^{-1}\right)+\frac{\partial}{\partial x}\left(\frac{\beta_s}{2}h_s(h_s+h_f)\right)=0,\quad \frac{\partial \hat{Q}_f}{\partial t}+\frac{\partial}{\partial y}\left(\hat{Q}_f^2 h_f^{-1}\right)+\frac{\partial}{\partial y}\left(\frac{\beta_f}{2}h_f(h_f+h_s)\right)=0. \tag{6}$$

Now, we replace $\hat{Q}_s=\hat{u}_s h_s$ and $\hat{Q}_f=\hat{u}_f h_f$. For notational brevity, from now on, we introduce the suffices $1:=s$ and $2:=f$ for the variables and parameters associated with the solid and fluid components respectively. Also, without loss of generality, we drop the hats: $(*):=(\hat{*})$. Then, (5) and (6) result in

$$\frac{\partial h_1}{\partial t}+\frac{\partial(u_1 h_1)}{\partial x}=0,\quad \frac{\partial h_2}{\partial t}+\frac{\partial(u_2 h_2)}{\partial y}=0, \tag{7}$$

$$\frac{\partial u_1}{\partial t}+u_1\frac{\partial u_1}{\partial x}+\beta_1\frac{\partial h_1}{\partial x}+\frac{\beta_1}{2}\frac{\partial h_2}{\partial x}+\frac{\beta_1}{2}\frac{h_2}{h_1}\frac{\partial h_1}{\partial x}=0,\quad \frac{\partial u_2}{\partial t}+u_2\frac{\partial u_2}{\partial y}+\beta_2\frac{\partial h_2}{\partial y}+\frac{\beta_2}{2}\frac{\partial h_1}{\partial y}+\frac{\beta_2}{2}\frac{h_1}{h_2}\frac{\partial h_2}{\partial y}=0. \tag{8}$$

Our model (7) and (8), as deduced from the mixture model in [1], are fundamentally new and different from the existing models. The fourth and fifth terms associated with $\beta/2$ in (8) that emerge from the pressure-gradients include buoyancy (through $1-\gamma$), friction (through K, and $\tan\delta$), net driving forces (S_s, S_f) and the coordinate transformations (4) that incorporate gravity, friction and buoyancy. These forces are mechanically important in explaining the physics of the two-phase gravity mass flows but are not considered in the previous models as done here for the mixture flows in connection to the application of Lie group. Importantly, these interacting (non-linear phase-interactions) pose great challenges in constructing exact solutions as compared to the effectively single-phase gravity mass flows. So, the problem we are considering here is fundamentally novel.

3. Calculation of the symmetry Lie algebra

There are two key steps in using the Lie symmetry method to study a system of PDEs. First, one computes the most general symmetry Lie group G or the symmetry Lie algebra $\mathfrak{g}$ of the system of PDEs, and then one uses the symmetries to reduce the system into a simpler system [19,23,28]. In this section, we focus on the symmetry Lie algebra $\mathfrak{g}$.

Let V be an element of $\mathfrak{g}$. It is also known as an infinitesimal symmetry. Our goal is to find all possible values of V. As our system has three independent variables x, y, t and four dependent variables h_1, h_2, u_1, u_2, a general element V of $\mathfrak{g}$ has the form

$$V=\xi_1\frac{\partial}{\partial x}+\xi_2\frac{\partial}{\partial y}+\xi_3\frac{\partial}{\partial t}+\eta_1\frac{\partial}{\partial h_1}+\eta_2\frac{\partial}{\partial h_2}+\eta_3\frac{\partial}{\partial u_1}+\eta_4\frac{\partial}{\partial u_2}, \tag{9}$$

where ξ_i and η_j $(i=1,2,3$ and $j=1,2,3,4)$ are respectively functions of independent and dependent variables [19,23,28]. As our system (7) and (8) is a first order system, we only need to consider the first prolongation $\mathrm{Pr}^1(V)$ of V [19,23,28]:

$$\begin{aligned}\mathrm{Pr}^1(V)=V&+\eta_1^x\frac{\partial}{\partial h_{1_x}}+\eta_1^y\frac{\partial}{\partial h_{1_y}}+\eta_1^t\frac{\partial}{\partial h_{1_t}}+\eta_2^x\frac{\partial}{\partial h_{2_x}}+\eta_2^y\frac{\partial}{\partial h_{2_y}}+\eta_2^t\frac{\partial}{\partial h_{2_t}}\\&+\eta_3^x\frac{\partial}{\partial u_{1_x}}+\eta_3^y\frac{\partial}{\partial u_{1_y}}+\eta_3^t\frac{\partial}{\partial u_{1_t}}+\eta_4^x\frac{\partial}{\partial u_{2_x}}+\eta_4^y\frac{\partial}{\partial u_{2_y}}+\eta_4^t\frac{\partial}{\partial u_{2_t}},\end{aligned} \tag{10}$$

where

$$\begin{aligned}\eta_1^x:=&(\eta_{1_x}+h_{1_x}\eta_{1_{h_1}}+h_{2_x}\eta_{1_{h_2}}+u_{1_x}\eta_{1_{u_1}}+u_{2_x}\eta_{1_{u_2}})-h_{1_x}(\xi_{1_x}+\xi_{1_{h_1}}h_{1_x}\\&+\xi_{1_{h_2}}h_{2_x}+\xi_{1_{u_1}}u_{1_x}+\xi_{1_{u_2}}u_{2_x})-h_{1_y}(\xi_{2_x}+\xi_{2_{h_1}}h_{1_x}+\xi_{2_{h_2}}h_{2_x}+\xi_{2_{u_1}}u_{1_x}\\&+\xi_{2_{u_2}}u_{2_x})-h_{1_t}(\xi_{3_x}+\xi_{3_{h_1}}h_{1_x}+\xi_{3_{h_2}}h_{2_x}+\xi_{3_{u_1}}u_{1_x}+\xi_{3_{u_2}}u_{2_x}),\end{aligned}$$

$$\begin{aligned}\eta_2^x:=&(\eta_{2_x}+h_{1_x}\eta_{2_{h_1}}+h_{2_x}\eta_{2_{h_2}}+u_{1_x}\eta_{2_{u_1}}+u_{2_x}\eta_{2_{u_2}})-h_{2_x}(\xi_{1_x}+\xi_{1_{h_1}}h_{1_x}\\&+\xi_{1_{h_2}}h_{2_x}+\xi_{1_{u_1}}u_{1_x}+\xi_{1_{u_2}}u_{2_x})-h_{2_y}(\xi_{2_x}+\xi_{2_{h_1}}h_{1_x}+\xi_{2_{h_2}}h_{2_x}+\xi_{2_{u_1}}u_{1_x}\\&+\xi_{2_{u_2}}u_{2_x})-h_{2_t}(\xi_{3_x}+\xi_{3_{h_1}}h_{1_x}+\xi_{3_{h_2}}h_{2_x}+\xi_{3_{u_1}}u_{1_x}+\xi_{3_{u_2}}u_{2_x}),\end{aligned}$$

$$\begin{aligned}\eta_3^x:=&(\eta_{3_x}+h_{1_x}\eta_{3_{h_1}}+h_{2_x}\eta_{3_{h_2}}+u_{1_x}\eta_{3_{u_1}}+u_{2_x}\eta_{3_{u_2}})-u_{1_x}(\xi_{1_x}+\xi_{1_{h_1}}h_{1_x}\\&+\xi_{1_{h_2}}h_{2_x}+\xi_{1_{u_1}}u_{1_x}+\xi_{1_{u_2}}u_{2_x})-u_{1_y}(\xi_{2_x}+\xi_{2_{h_1}}h_{1_x}+\xi_{2_{h_2}}h_{2_x}\\&+\xi_{2_{u_1}}u_{1_x}+\xi_{2_{u_2}}u_{2_x})-u_{1_t}(\xi_{3_x}+\xi_{3_{h_1}}h_{1_x}+\xi_{3_{h_2}}h_{2_x}+\xi_{3_{u_1}}u_{1_x}+\xi_{3_{u_2}}u_{2_x}),\end{aligned}$$

$$\begin{aligned}\eta_4^x:=&(\eta_{4_x}+h_{1_x}\eta_{4_{h_1}}+h_{2_x}\eta_{4_{h_2}}+u_{1_x}\eta_{4_{u_1}}+u_{2_x}\eta_{4_{u_2}})-u_{2_x}(\xi_{1_x}+\xi_{1_{h_1}}h_{1_x}\\&+\xi_{1_{h_2}}h_{2_x}+\xi_{1_{u_1}}u_{1_x}+\xi_{1_{u_2}}u_{2_x})-u_{2_y}(\xi_{2_x}+\xi_{2_{h_1}}h_{1_x}+\xi_{2_{h_2}}h_{2_x}+\xi_{2_{u_1}}u_{1_x}\\&+\xi_{2_{u_2}}u_{2_x})-u_{2_t}(\xi_{3_x}+\xi_{3_{h_1}}h_{1_x}+\xi_{3_{h_2}}h_{2_x}+\xi_{3_{u_1}}u_{1_x}+\xi_{3_{u_2}}u_{2_x}).\end{aligned}$$

Here, the expression with subscripts x, y, t, h_1, h_2, u_1 and u_2 means the partial derivatives, for example, the notation η_{1x} means $\partial\eta_1/\partial x$. Replacing x by y and t for the terms inside the parenthesis, we get the η_j^y and η_j^t respectively.

A vector field V as in (9) is an infinitesimal symmetry if it satisfies the prolongation condition [28]. So, we apply the prolongation (10) to the system (7) and (8) and then equate each of these expressions to zero. This process results in a set of four equations. Now, using the functional independence of the partial derivatives of $\xi_1, \xi_2, \xi_3, \eta_1, \eta_2, \eta_3$ and η_4, we get a set of partial differential equations for $\xi_1, \xi_2, \xi_3, \eta_1, \eta_2, \eta_3$ and η_4 which are called the determining equations. The solutions of the determining equations compute all the possible infinitesimal symmetries and hence the desired symmetry Lie algebra $\mathfrak{g}$.

Following routine computations, we compute the solutions of the determining equations of the system (7) and (8):

$$\xi_1=p_1x+q_1,\quad \xi_2=p_2y+q_2,\quad \xi_3=p_3t+q_3, \tag{11}$$

$$\eta_1=2(p_1-p_3)h_1,\quad \eta_2=2(p_1-p_3)h_2,\quad \eta_3=(p_1-p_3)u_1,\quad \eta_4=(p_1-p_3)u_2, \tag{12}$$

where p_i and q_j are constants and $p_1=p_2$. It is important to note

$p_1 = p_2$, it shows the stretching of x and y in ξ_1 and ξ_2 are same. This is expected as x and y are defined in (4) with the same base variable X and they only differ by translations depending on S_s and S_f respectively, which corresponds to q_1 and q_2.

Therefore, an arbitrary element V of $\mathfrak{g}$ has the form

$$V = q_1V_1 + q_2V_2 + q_3V_3 + p_1V_4 + + p_3V_5,$$

where

$$V_1 = \frac{\partial}{\partial x}, \quad V_2 = \frac{\partial}{\partial y}, \quad V_3 = \frac{\partial}{\partial t}, \quad V_4 = x\frac{\partial}{\partial x} + y\frac{\partial}{\partial y} + 2h_1\frac{\partial}{\partial h_1} + 2h_2\frac{\partial}{\partial h_2} + u_1\frac{\partial}{\partial u_1} + u_2\frac{\partial}{\partial u_2} \text{ and}$$

$$V_5 = t\frac{\partial}{\partial t} - 2h_1\frac{\partial}{\partial h_1} - 2h_2\frac{\partial}{\partial h_2} - u_1\frac{\partial}{\partial u_1} - u_2\frac{\partial}{\partial u_2}. \tag{13}$$

This shows that $\mathfrak{g}$ is a five dimensional vector space with a basis $\{V_1, V_2, V_3, V_4, V_5\}$. In fact, $\mathfrak{g}$ is a Lie algebra. We can directly compute the Lie bracket on this basis: $[V_1, V_4] = V_1, [V_2, V_4] = V_2, [V_3, V_5] = V_3$, and $[V_i, V_j] = 0$ for the remaining cases (see Table 1). In summary,

Theorem. *The symmetry Lie algebra $\mathfrak{g}$ of the system (7) and (8) is a five dimensional Lie algebra spanned by V_1, V_2, V_3, V_4 and V_5 from (13) with the Lie bracket operation as shown in Table 1.*

4. Similarity reduced equations

Next, we reduce the system (7) and (8) into a possibly easier system or analytically solvable system [19,23,28]. The main idea here is to look for certain type of solutions which are invariant under certain symmetry. This is done by introducing similarity variables and similarity forms with the aid of the infinitesimal symmetries. A similarity variable is a new independent variable for the reduced forms of the original system, which can be determined by integrating terms of the characteristic equation [27] associated to the independent variables, for example, the terms associated with the time and space variables. Similarly, the similarity forms (new dependent variables) can be obtained by integrating the differential terms in the characteristic equation associated with time and each dynamical variable, or space and each dynamical variable. Finally, the reduced system of equations is obtained in terms of the similarity variables and the dependent similarity forms by substituting them into the original system of equations.

Let us consider the infinitesimal symmetry $\tilde{V} = \frac{\partial}{\partial x} - \frac{\partial}{\partial y} \in \mathfrak{g}$. Although, this is one of the most simple elements in $\mathfrak{g}$, we will see, this has several interesting and important consequences. The characteristics equation of $\tilde{V}$ is $\frac{dx}{1} = \frac{dy}{-1}$. Integrating this equation, we get $x + y = w$, where the parameter w emerges from integration. Hence, the similarity variables are $w = x + y$ and t. The similarity forms $\hat{u}_1, \hat{u}_2, \hat{h}_1$ and $\hat{h}_2$ are given by

$$h_1(x,y,t) = \hat{h}_1(w,t), \quad u_1(x,y,t) = \hat{u}_1(w,t); \quad h_2(x,y,t) = \hat{h}_2(w,t), \quad u_2(x,y,t) = \hat{u}_2(w,t).$$

Now substituting $\hat{h}_1, \hat{h}_2, \hat{u}_1$ and $\hat{u}_2$ into the system (7) and (8), and using the chain rule, we obtain

$$\frac{\partial \hat{h}_1}{\partial t} + \frac{\partial(\hat{u}_1\hat{h}_1)}{\partial w} = 0, \quad \frac{\partial \hat{h}_2}{\partial t} + \frac{\partial(\hat{u}_2\hat{h}_2)}{\partial w} = 0, \tag{14}$$

$$\frac{\partial \hat{u}_1}{\partial t} + \hat{u}_1\frac{\partial \hat{u}_1}{\partial w} + \beta_1\frac{\partial \hat{h}_1}{\partial w} + \frac{\beta_1}{2}\frac{\partial \hat{h}_2}{\partial w} + \frac{\beta_1}{2}\frac{\hat{h}_2}{\hat{h}_1}\frac{\partial \hat{h}_1}{\partial w} = 0, \quad \frac{\partial \hat{u}_2}{\partial t} + \hat{u}_2\frac{\partial \hat{u}_2}{\partial w} + \beta_2\frac{\partial \hat{h}_2}{\partial w} + \frac{\beta_2}{2}\frac{\partial \hat{h}_1}{\partial w} + \frac{\beta_2}{2}\frac{\hat{h}_1}{\hat{h}_2}\frac{\partial \hat{h}_2}{\partial w} = 0, \tag{15}$$

in which the spatial variable is reduced to one, i.e., w.

Taking a similar approach, we find (14) and (15) has a four dimensional symmetry Lie subalgebra $\mathfrak{h}$ spanned by X_1, X_2, X_3, X_4, where

$$X_1 = \frac{\partial}{\partial w}, \quad X_2 = \frac{\partial}{\partial t}, \quad X_3 = w\frac{\partial}{\partial w} + 2\hat{h}_1\frac{\partial}{\partial \hat{h}_1} + 2\hat{h}_2\frac{\partial}{\partial \hat{h}_2} + \hat{u}_1\frac{\partial}{\partial \hat{u}_1} + \hat{u}_2\frac{\partial}{\partial \hat{u}_2} \text{ and}$$

$$X_4 = t\frac{\partial}{\partial t} - 2\hat{h}_1\frac{\partial}{\partial \hat{h}_1} - 2\hat{h}_2\frac{\partial}{\partial \hat{h}_2} - \hat{u}_1\frac{\partial}{\partial \hat{u}_1} - \hat{u}_2\frac{\partial}{\partial \hat{u}_2}$$

are infinitesimal symmetries. Table 2 shows the Lie bracket operation on this basis.

Let X be an arbitrary element of the symmetry Lie subalgebra $\mathfrak{h}$. Then, we can write

$$X = (a_1 + a_3w)\frac{\partial}{\partial w} + (a_2 + a_4t)\frac{\partial}{\partial t} + 2(a_3 - a_4)\hat{h}_1\frac{\partial}{\partial \hat{h}_1} + 2(a_3 - a_4)\hat{h}_2\frac{\partial}{\partial \hat{h}_2} + (a_3 - a_4)\hat{u}_1\frac{\partial}{\partial \hat{u}_1} + (a_3 - a_4)\hat{u}_2\frac{\partial}{\partial \hat{u}_2},$$

where a_1, a_2, a_3, and a_4 are parameters of the Lie subalgebra of the infinitesimal symmetries. Different choices of the parameters give different similarity variables, similarity forms, and finally different reduced models and their respective solutions representing the solutions of the given system that preserve symmetry.

The characteristic equation for X [27] is

$$\frac{dw}{a_1 + a_3w} = \frac{dt}{a_2 + a_4t} = \frac{d\hat{h}_1}{2(a_3 - a_4)\hat{h}_1} = \frac{d\hat{h}_2}{2(a_3 - a_4)\hat{h}_2} = \frac{d\hat{u}_1}{(a_3 - a_4)\hat{u}_1} = \frac{d\hat{u}_2}{(a_3 - a_4)\hat{u}_2}. \tag{16}$$

The above characteristics equation associated with the subalgebra $\mathfrak{h}$ generalizes several subalgebras considered in [11]. Here, this subalgebra is associated with the two-phase gravity mass flows in inclined channel that includes gravity, friction, pressure-gradients, buoyancy and phase-interactions.

We will use (16) to reduce the PDEs (14) and (15) to several systems of ordinary differential equations (ODEs). For simplicity, we define

$$l := (a_3 - a_4)/a_4, \; m := (a_4 + a_3)/a_4, \; n := (a_3 - a_4)/a_3,$$

$$p := (a_1 + a_4)/a_1 \quad \text{and} \quad q := (a_2 + a_3)/a_3.$$

5. Reduction to system of ODEs and analysis—a homogeneous model

In this section, we derive and analyze a reduced homogeneous model. For this we suppose $a_3 = a_4 = 0$ and $a_1, a_2 \neq 0$. Integrating the first two terms of (16) gives the similarity variable, v:

$$v = a_2w - a_1t. \tag{18}$$

The corresponding similarity forms $\tilde{h}_1, \tilde{h}_2, \tilde{u}_1$, and $\tilde{u}_2$ are given by

$$\hat{h}_1(w,t) = \tilde{h}_1(v), \quad \hat{u}_1(w,t) = \tilde{u}_1(v); \quad \hat{h}_2(w,t) = \tilde{h}_2(v), \quad \hat{u}_2(w,t) = \tilde{u}_2(v). \tag{19}$$

With (19), (14) and (15) reduces to the homogeneous system of ODEs:

$$\begin{bmatrix} -a_1 + a_2\tilde{u}_1 & 0 & a_2\tilde{h}_1 & 0 \\ 0 & -a_1 + a_2\tilde{u}_2 & 0 & a_2\tilde{h}_2 \\ \beta_1a_2 + 0.5\beta_1a_2\tilde{h}_2/\tilde{h}_1 & 0.5\beta_1a_2 & -a_1 + a_2\tilde{u}_1 & 0 \\ 0.5\beta_2a_2 & \beta_2a_2 + 0.5\beta_2a_2\tilde{h}_1/\tilde{h}_2 & 0 & -a_1 + a_2\tilde{u}_2 \end{bmatrix} \begin{bmatrix} d\tilde{h}_1/dv \\ d\tilde{h}_2/dv \\ d\tilde{u}_1/dv \\ d\tilde{u}_2/dv \end{bmatrix} = \begin{bmatrix} 0 \\ 0 \\ 0 \\ 0 \end{bmatrix}. \tag{20}$$

So, the non-stretching of the time and space (i.e., $a_3 = 0 = a_4$) generates homogeneous ODEs for the similarity forms implicitly in similarity variables.

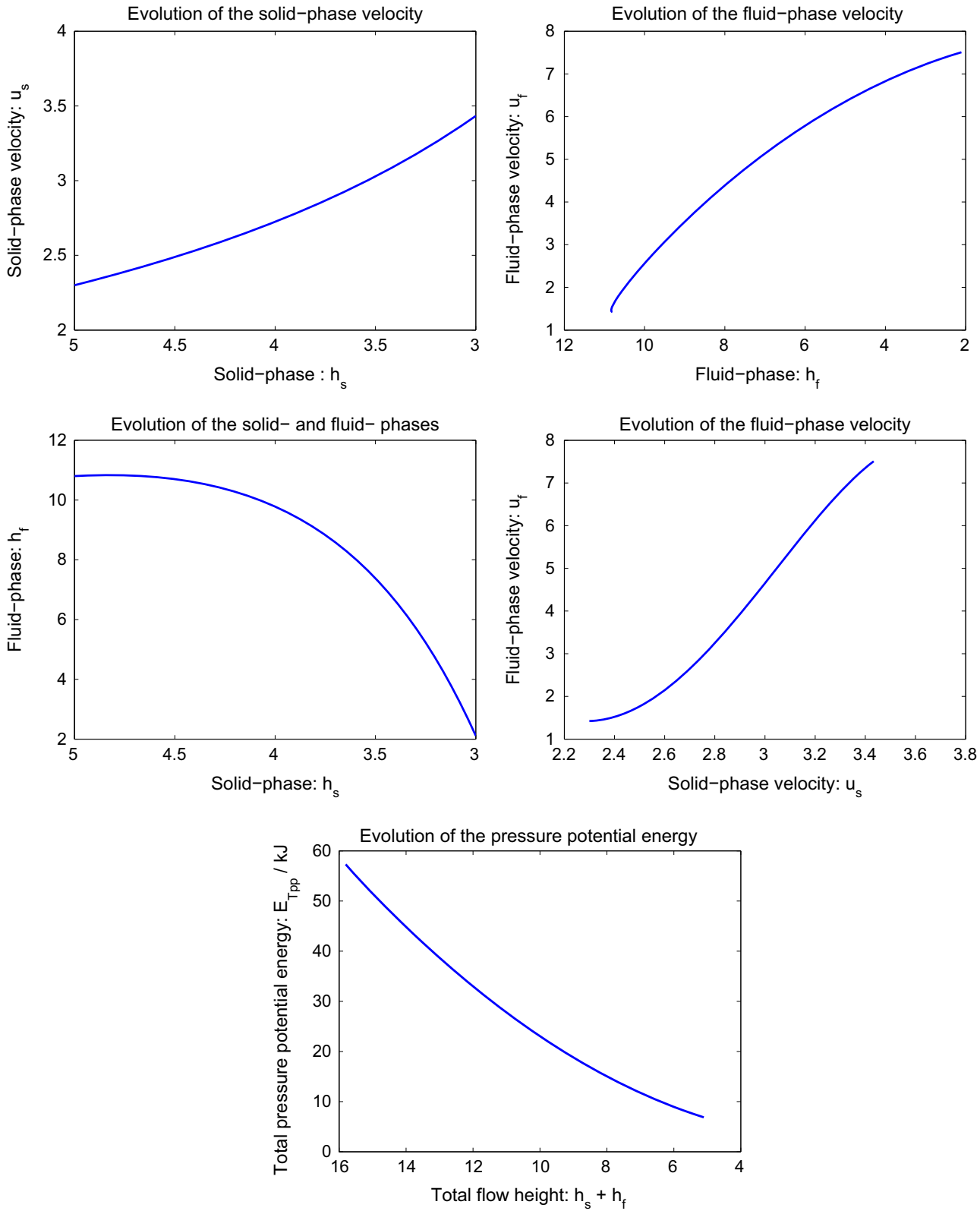

Fig. 1. Dynamics and interactions of the solid- and fluid-phase velocities and heights, and the total pressure potential energy as given by the solution (27) as derived by solving the reduced system (20).

The first and third rows in (20) result in the following mass and momentum balances for the solid-phase:

$$\frac{d}{dv}\left[-a_1\tilde{h}_1+a_2\tilde{h}_1\tilde{u}_1\right]=0,\quad \frac{d}{dv}\left[-a_1\tilde{h}_1\tilde{u}_1+a_2\tilde{h}_1\tilde{u}_1^2+\frac{\beta_1}{2}a_2\tilde{h}_1^2+\frac{\beta_1}{2}a_2\tilde{h}_1\tilde{h}_2\right]=0. \tag{21}$$

Eq. $(21)_2$ is obtained by utilizing the solid-mass balance equation (the first row in (20)). In $(21)_2$ the first, second, third and fourth terms are associated with the solid mass flux, solid momentum flux, hydraulic pressure gradient for solid, and the hydraulic pressure gradient enhanced by phase-interaction respectively. Eq. (21) can be solved analytically to yield the exact solutions:

$$-a_1\tilde{h}_1+a_2\tilde{h}_1\tilde{u}_1=\lambda_{1_m},\quad -a_1\tilde{h}_1\tilde{u}_1+a_2\tilde{h}_1\tilde{u}_1^2+\frac{\beta_1}{2}a_2\tilde{h}_1\left(\tilde{h}_1+\tilde{h}_2\right)=\lambda_{1_M}, \tag{22}$$

where λ_{1_m} and λ_{1_M} are constants of integration whose values can be constrained, e.g., from experiments, by knowing the mass and momentum fluxes at some instants/locations [40]. Similarly, a system of exact solutions can be obtained for the fluid-phase:

$$-a_1\tilde{h}_2+a_2\tilde{h}_2\tilde{u}_2=\lambda_{2_m},\quad -a_1\tilde{h}_2\tilde{u}_2+a_2\tilde{h}_2\tilde{u}_2^2+\frac{\beta_2}{2}a_2\tilde{h}_2\left(\tilde{h}_2+\tilde{h}_1\right)=\lambda_{2_M}, \tag{23}$$

where λ_{2_m} and λ_{2_M} are constants of integration whose values can be constrained as mentioned above. The system (22) and (23) constituting the solutions to the ODE system (20) is non-linear in $(\tilde{h}_1,\tilde{h}_2;\tilde{u}_1,\tilde{u}_2)$. So, most probably it is not possible to explicitly and fully express solutions for $\tilde{h}_1,\tilde{h}_2;\tilde{u}_1,\tilde{u}_2$ in terms of the involved parameters $a_1,a_2;\beta_1,\beta_2;\lambda_{1_m},\lambda_{1_M};\lambda_{2_m},\lambda_{2_M}$. In the sequel, we discuss some special situations for (22) and (23).

$\tilde{h}_1=\tilde{h}_2$: In this special situation, the system (22) and (23) are decoupled. Then (22) implies the solution for the solid-phase velocity and flow height (similarly, (23) provides analogous solutions for the fluid-phase):

$$(\lambda_{1_m}a_2^2)\tilde{u}_1^3-(2a_1a_2\lambda_{1_m}-a_2^2\lambda_{1_M})\tilde{u}_1^2+(a_1^2\lambda_{1_m}+2a_1a_2\lambda_{1_M})\tilde{u}_1+\left(\beta_1a_2\lambda_{1_m}^2-a_1^2\lambda_{1_M}\right)=0,\quad \tilde{h}_1=\lambda_{1_m}/(-a_1+a_2\tilde{u}_1). \tag{24}$$

$\tilde{h}_1=0$ *or* $\tilde{h}_2=0$: Note that $\tilde{h}_2=0$ results in classical single-phase solution for solid, which is obtained from (24) by replacing β_1 by $\beta_1/2$. Analogously, $\tilde{h}_1=0$ provides classical single-phase solution for fluid.

Neutrally buoyant flow: Let $\gamma=1$, $\beta_1=0$. Then (22) results in a simple system consisting of only $\tilde{h}_1$ and $\tilde{u}_1$. So, the solution for the solid is

$$\tilde{u}_1=\lambda_1,\quad \tilde{h}_1=\lambda_{1_m}/(-a_1+a_2\lambda_1), \tag{25}$$

where $\lambda_1=\lambda_{1_M}/\lambda_{1_m}$. With this, the solutions for the fluid velocity and height yield

$$\tilde{u}_2=\left(\lambda_{2_M}-\frac{\beta_2}{2}a_2\tilde{h}_2\left(\tilde{h}_2+\tilde{\lambda}_1\right)\right)/\lambda_{2_m},\quad \tilde{h}_2^3+\tilde{\lambda}_1\tilde{h}_2^2+\frac{2}{\beta_2a_2^2}(a_1\lambda_{2_m}-a_2\lambda_{2_M})\tilde{h}_2+\frac{2\lambda_{2_m}^2}{\beta_2a_2^2}=0, \tag{26}$$

where $\tilde{\lambda}_1=\lambda_{1_m}^2/(-a_1\lambda_{1_m}+a_2\lambda_{1_M})$. Eq. (26) is cubic in $\tilde{h}_2$ and $\tilde{u}_2$ is quadratic in $\tilde{h}_2$. This means that as $\tilde{h}_2$ decreases $\tilde{u}_2$ increases quadratically for appropriately chosen parameters $a_1,a_2;\lambda_{1_m},\lambda_{1_M};\lambda_{2_m},\lambda_{2_M};\beta_1,\beta_2$. Such quadratic solutions are observed in real flow situations [10].

General solutions: Assume that the solid flow height $\tilde{h}_1$ is known (say from experiments or observation). Then from (22) and (23), the general solutions for $\tilde{u}_1$, $\tilde{h}_2$ and $\tilde{u}_2$ can be constructed explicitly in terms of $\tilde{h}_1$ and other physical parameters of the model equations:

$$\tilde{u}_1=\frac{\lambda_{1_m}+a_1\tilde{h}_1}{a_2\tilde{h}_1},\quad \tilde{h}_2=\frac{2}{\beta_1a_2^2\tilde{h}_1^2}\left[\lambda_{1_M}a_2\tilde{h}_1-\lambda_{1_m}\left(\lambda_{1_m}+a_1\tilde{h}_1\right)-\beta_1a_2^2\tilde{h}_1^3\right],\quad \tilde{u}_2=\frac{1}{\lambda_{2_m}}\left[\lambda_{2_M}-\frac{1}{2}\beta_2a_2\tilde{h}_2\left(\tilde{h}_2+\tilde{h}_1\right)\right]. \tag{27}$$

Solutions (27) are plotted in Fig. 1 for velocity, flow height and pressure potential energy to the two-phase mass flows as a mixture of solid particles and fluid. The chosen parameter values are $a_1=6, a_2=10; \beta_1=0.3025, \beta_2=0.4565; \lambda_{1_m}=85, \lambda_{1_M}=315; \lambda_{2_m}=60, \lambda_{2_M}=475$. The solid and fluid densities are $\rho_1=2700$ and $\rho_2=1100$ respectively [1]. The energy equations are derived from the momentum balances. These solutions are extensions to the previously obtained solutions for single-phase flows, such as granular and debris flows. The solutions reveal strong solid–fluid phase interactions, and non-linear relationships between the flow dynamical variables, the solid- and fluid-heights and solid- and fluid-phase velocities $(h_s,h_f;u_s,u_f)$. These results correspond to the situation of continuous and uniform mass release from a reservoir or silo [10,40]. After the release of the debris mixture, both the solid and the fluid masses rarefy resulting in the decrease of the solid and the fluid heights along the down-slope direction. As both the solid and the fluid mass accelerate down-slope, the corresponding solid- and fluid-phase velocities increase. There are several important relationships between the flow heights and velocities. Although, the flow velocities vary quadratically with the corresponding phase-flow heights, solid phase-velocity (u_s) varies concavely with the solid phase height (h_s) whereas this relationship is convex for fluid phase. Similarly, the solid and fluid heights and the solid and the fluid phase velocities vary strongly non-linearly.

6. Reduction to system of ODEs and analysis—non-homogeneous model I

Now, we deal with the full models. Using (16) solutions of the system, (14) and (15) could not be derived explicitly and fully in terms of the similarity variables and finally in terms of the physical variables. Such system and solutions can only be developed/obtained by considering some special choices of time and/or spatial stretching parameters and the dynamics associated with such parameters.

First, we suppose $a_3\neq 0$ and $a_4\neq 0$. In this case, the similarity variable is

$$v=(a_2+a_4t)(a_1+a_3w)^{-a_4/a_3}. \tag{28}$$

6.1. Similarity form associated with time element (operator)

Integrating the equations consisting of second and third, second and fourth, second and fifth, second and sixth expressions respectively in (16), we get the similarity forms $(\tilde{h}_1,\tilde{h}_2;\tilde{u}_1,\tilde{u}_2)$:

$$\hat{h}_1(w,t)=(a_2+a_4t)^{2l}\tilde{h}_1(v),\quad \hat{u}_1(w,t)=(a_2+a_4t)^{l}\tilde{u}_1(v);$$
$$\hat{h}_2(w,t)=(a_2+a_4t)^{2l}\tilde{h}_2(v),\quad \hat{u}_2(w,t)=(a_2+a_4t)^{l}\tilde{u}_2(v). \tag{29}$$

Inserting the similarity forms (29) in (14) and (15), we obtain a system of ODEs:

$$\begin{bmatrix} v-v^m\tilde{u}_1 & 0 & -v^m\tilde{h}_1 & 0\\ 0 & v-v^m\tilde{u}_2 & 0 & -v^m\tilde{h}_2\\ -\beta_1v^m-0.5\beta_1v^m\tilde{h}_2/\tilde{h}_1 & -0.5\beta_1v^m & v-v^m\tilde{u}_1 & 0\\ -0.5\beta_2v^m & -\beta_2v^m-0.5\beta_2v^m\tilde{h}_1/\tilde{h}_2 & 0 & v-v^m\tilde{u}_2 \end{bmatrix}$$

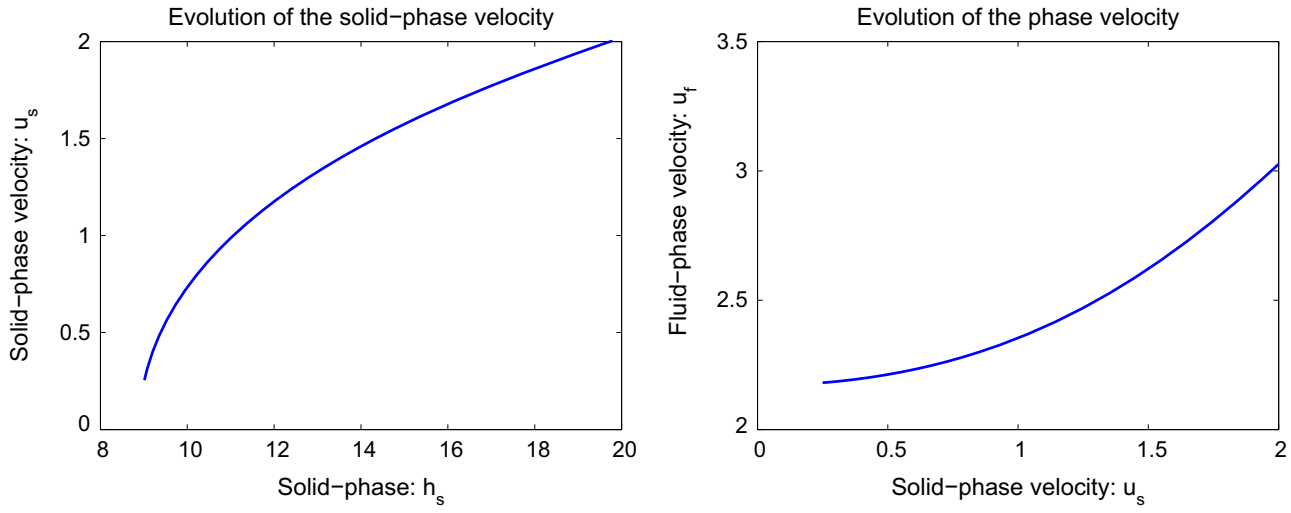

Fig. 2. Relationship between solid height and velocity, and solid- and fluid-phase velocities (34) as derived by solving reduced system (30).

$$\begin{bmatrix} d\tilde{h}_1/dv \\ d\tilde{h}_2/dv \\ d\tilde{u}_1/dv \\ d\tilde{u}_2/dv \end{bmatrix} = \begin{bmatrix} -2l\tilde{h}_1 \\ -2l\tilde{h}_2 \\ -l\tilde{u}_1 \\ -l\tilde{u}_2 \end{bmatrix}. \tag{30}$$

Interestingly, solutions of the flow heights $(\hat{h}_1, \hat{h}_2)$ are $2l$ time-exponent multiple of the similarity forms $\tilde{h}_1, \tilde{h}_2$, whereas this relation is l time-exponent multiple of the similarity forms $\tilde{u}_1, \tilde{u}_2$ for the flow velocities $(\hat{u}_1, \hat{u}_2)$.

6.1.1. Exact solutions for reduced form

Explicit exact solutions can be constructed for $a_3 = a_4$. Since $l = a_3/a_4 - 1$, (29) shows the similarity forms $(\tilde{h}_1, \tilde{h}_2\ ;\ \tilde{u}_1, \tilde{u}_2)$ are the required solutions $(\hat{h}_1, \hat{h}_2\ ;\ \hat{u}_1, \hat{u}_2)$ associated with the similarity variable $v = (a_2 + a_3 t)/(a_1 + a_3 w)$. In this limiting situation $(l = 0, m = 2)$, the system (30) becomes homogeneous, and for sufficiently large v, the solid (similarly the fluid) mass and momentum balances, can be combined to obtain

$$-\tilde{h}_1\tilde{u}_1^2 + \tfrac{1}{2}\beta_1\tilde{h}_1\left(\tilde{h}_1 + \tilde{h}_2\right) = \lambda_1, \quad -\tilde{h}_2\tilde{u}_2^2 + \tfrac{1}{2}\beta_2\tilde{h}_2\left(\tilde{h}_2 + \tilde{h}_1\right) = \lambda_2, \tag{31}$$

where λ_1 and λ_2 are constants of integration.

In real applications, the values of λ_1, λ_2 can be determined from the physics of the problem, e.g., the boundary conditions. In particular, $\lambda_1 = 0$ and $\lambda_2 = 0$ implies

$$\tilde{u}_1 = \sqrt{\beta_1/\beta_2}\,\tilde{u}_2. \tag{32}$$

This indicates that for the problem considered here the pressure-gradient parameters play dominant role to reveal that in the real two-phase flows phase-velocities are not the same, i.e., $\tilde{u}_1 \neq \tilde{u}_2$. For larger solid pressure-gradient than the fluid $(\beta_1 > \beta_2)$, the solid velocity dominates the fluid velocity and vice versa. They coincide only if $\beta_1 = \beta_2$. These are intuitively clear phenomena for pressure driven flows. The novel solution (32) is technically important, because with this, one of the phase velocities can be obtained from the other and the known physical parameters of the mixture contained in β_1 and β_2. We will discuss more on the role of the parameters for the general solutions later.

In general, rearranging and dividing the first by the second in (31) we obtain

$$\frac{\tilde{h}_1\tilde{u}_1^2 + \lambda_1}{\tilde{h}_2\tilde{u}_2^2 + \lambda_2} = \frac{\beta_1}{\beta_2}\frac{\tilde{h}_1}{\tilde{h}_2} =: \frac{1}{\Omega}, \tag{33}$$

where $1/\Omega$ is the proportionality parameter. With this, we obtain the following set of explicit solutions for $\tilde{h}_1, \tilde{h}_2$, and $\tilde{u}_2$ in terms of $\tilde{u}_1$ (other sets of equivalent solutions are possible):

$$\tilde{h}_1 = \frac{1}{\beta_1(1+\tilde{\Omega})}\left(\tilde{u}_1^2 \pm \sqrt{\tilde{u}_1^4 - 2\beta_1\left(1+\tilde{\Omega}\right)\lambda_1}\right), \quad \tilde{h}_2 = \tilde{\Omega}\tilde{h}_1, \quad \tilde{u}_2 = \sqrt{\frac{\beta_2}{2}\left(1+\tilde{\Omega}\right)\tilde{h}_1 + \frac{\lambda_1}{\tilde{h}_1}}, \tag{34}$$

where $\tilde{\Omega} = \Omega(\beta_1/\beta_2)$. In particular, for $\lambda_1 = 0$ we obtain $\tilde{h}_1 = 2\tilde{u}_1^2/\left(\beta_1\left(1+\tilde{\Omega}\right)\right)$, $\tilde{h}_2 = \tilde{\Omega}\tilde{h}_1$, $\tilde{u}_2 = \sqrt{\beta_2/\beta_1}\,\tilde{u}_1$. So, this recovers $\tilde{u}_1 = \sqrt{\beta_1/\beta_2}\,\tilde{u}_2$ in (32).

Fig. 2 represents evolutions of the solid-phase and fluid-phase velocities and heights as given by (34) for sufficiently large v, which can be realized by setting large time t. The parameters are $\lambda_1 = -20, \lambda_2 = -10; \beta_1 = 0.2025, \beta_2 = 0.3565, \quad \Omega = 1.5$. These results can be interpreted as follows. By fixing a downslope position, we see as the flow reaches this position the flow velocity increases quadratically as a function of the flow height. Interestingly, as the solid velocity at this position increases the fluid velocity also increases quadratically. The results presented in Figs. 1 and 2 are physically meaningful and can be observed phenomena in nature. Furthermore, for $a_4 \to 0, l \to -\infty$ produces far-field trivial solutions $\hat{h}_1 \to 0, \hat{h}_2 \to 0; \hat{u}_1 \to 0, \hat{u}_2 \to 0$ corresponding to the similarity variable $v = a_2$.

6.1.2. Numerical solutions for general form

For general parameters, the system (30) has been solved numerically and the results are presented in Fig. 4 for the parameters $a_1 = 0.5, a_2 = -7.0; a_3 = 5.0, a_4 = 5.45; \beta_1 = 0.32, \beta_2 = 0.22; t \in (0.01, 1.1), w \in (0.01, 1.1)$. The mixture mass consisting of 50% solid and 50% fluid is fed continuously and uniformly from the left boundary. The solutions are associated with the arc corresponding to $t = 1.1$ on the manifold v of similarity variable (Fig. 3).

These solutions correspond to the physical problem of rapid flows of a two-phase mixture of solid particles and the viscous fluid down a slope released from a reservoir. Fig. 4 shows the phase-flow heights (panel (a)) and velocities (panel (b)) in terms of the similarity variable v, phase-flow heights and velocities in terms of the physical variables x (panels (c) and (d)) and the phase-flow heights and velocities in terms of the physical variable X (panels (e) and (f)) with $S_s = 0.50$ and $S_f = 0.75$ corresponding to the channel inclination of 45°. Due to the friction and buoyancy reduced load of the solid particles, the net driving force for the solid (S_s) is less than the net driving force for the fluid phase (S_f).

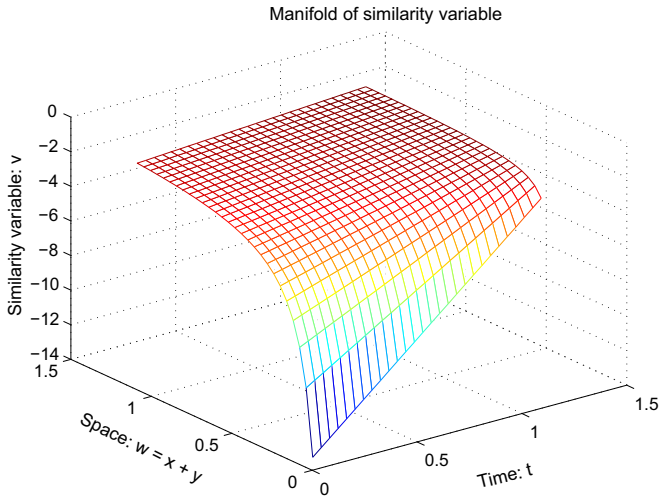

Fig. 3. The manifold ν given by (28) for the parameter choice: $a_1=0.5, a_2=-7.0; a_3=5.0, a_4=5.45$.

As the flow propagates down slope, due to shearing, the flow thickness decreases whereas due to the flow in the inclined channel, the velocities increase. Importantly, although the boundary conditions for the solid and fluid heights and solid and fluid velocities on the left of the computational domain are the same, they evolve fundamentally differently. As the flow cascades down slope, the solid-phase flow depth decreases faster than the fluid-phase flow depth. This resulted in the higher flow velocity of the solid-phase as compared to the fluid-phase velocity. Both the solid and the fluid phase velocities are increasing rapidly as the flow is released, then tend to slow down and somehow to attain steady-state. These solutions reveal strong non-linear and distinct evolutions of the solid and fluid phase dynamics (flow heights and flow velocities).

The role of pressure parameters for the system (30): Since the model equations (30) are strongly coupled by the pressure parameters β_1 and β_2 and the associated force due to the hydraulic pressure-gradients for the solid and the fluid, it is important to analyze the effect of these parameters in detail. For this purpose, we switch the pressure parameters: $\beta_2=0.32, \beta_1=0.22$. The results are presented in Fig. 5. The results are also just switched from solid to fluid from Fig. 4. Panel (e) and panel (f) are physically more relevant and particularly reveal further important aspects: (i) for certain downslope distance from the flow release the solid height dominates, then in the farther downstream, the fluid height takes over. (ii) Flow velocities show that the fluid-phase velocity dominates entirely. (iii) Both panels (e) and (f) show that the fluid-phase front is much farther than the solid-phase front. (iv) The dominance of the solid or the fluid velocity results mainly from the pressure parameter and the front position dominance by fluid (or solid) is determined by the net driving force, which in the present consideration is larger for the fluid. This is the reason for the farther downstream position of the fluid front than the solid front.

Such simultaneous and explicit solutions, as constructed by employing the Lie algebra, for the phase-heights and phase-velocities for the solid and fluid as the two-phase mixture material moves down-slope is novel. Although the solutions vary strongly non-linearly, they behave qualitatively similarly both in the similarity and physical variables. The most important aspects here are the following: (i) Non-linear and distinct evolutions of the solid and fluid phase dynamics (flow heights and flow velocities). Such solutions are possible only with real two-phase mass flow models. (ii) These flow behaviors are intuitively clear and observable physical phenomena in nature and industrial flows of mixture material down a slope. Nevertheless, it is not within the scope to validate these results.

Furthermore, we took the same pressure parameters $\beta_1=0.32$ and $\beta_2=0.32$. With this, the solutions for the solid and the fluid flow heights and flow velocities coincide (Fig. 6). These results show that phase-interactions are important and that our solutions derived with the Lie algebra symmetry produce physically relevant and consistent results.

6.2. *Similarity form associated with spatial element (operator)*

For the same similarity variable (28), we obtain another set of similarity forms by integrating the equations consisting of first and third, first and fourth, first and fifth, first and sixth expressions respectively in (16):

$$\hat{h}_1(w,t)=(a_1+a_3w)^{2n}\tilde{h}_1(\nu), \quad \hat{u}_1(w,t)=(a_1+a_3w)^n\tilde{u}_1(\nu);$$
$$\hat{h}_2(w,t)=(a_1+a_3w)^{2n}\tilde{h}_2(\nu), \quad \hat{u}_2(w,t)=(a_1+a_3w)^n\tilde{u}_2(\nu). \tag{35}$$

Substituting these into (14) and (15) we get an alternative set of ODEs to (30):

$$\begin{bmatrix} 1-\nu\tilde{u}_1 & 0 & -\nu\tilde{h}_1 & 0 \\ 0 & 1-\nu\tilde{u}_2 & 0 & -\nu\tilde{h}_2 \\ -\beta_1\nu-0.5\beta_1\tilde{h}_2/\tilde{h}_1 & -0.5\beta_1\nu & 1-\nu\tilde{u}_1 & 0 \\ -0.5\beta_2\nu & -\beta_2\nu-0.5\beta_2\tilde{h}_1/\tilde{h}_2 & 0 & 1-\nu\tilde{u}_2 \end{bmatrix}$$
$$\begin{bmatrix} d\tilde{h}_1/d\nu \\ d\tilde{h}_2/d\nu \\ d\tilde{u}_1/d\nu \\ d\tilde{u}_2/d\nu \end{bmatrix} = \begin{bmatrix} -3l\tilde{u}_1\tilde{h}_1 \\ -3l\tilde{u}_2\tilde{h}_2 \\ -l(\tilde{u}_1^2+2\beta_1(\tilde{h}_1+\tilde{h}_2)) \\ -l(\tilde{u}_2^2+2\beta_2(\tilde{h}_1+\tilde{h}_2)) \end{bmatrix}. \tag{36}$$

Structurally, (30) and (36) are similar. Nevertheless, cross-coupling and phase-interactions are explicit in (36) as evident from the right-hand-side vector which reveals the quadratic terms in velocity and flow depth and their sums. Another important aspect is that the parameter m is not present in the system matrix but the pressure parameters appear in the right-hand-side source vector.

Now, we analyze the solution for the model (36). The system is solved numerically and the results are presented in Fig. 8 for the parameters $a_1=1.0, a_2=-1.32; a_3=10.50, a_4=11.75; \beta_1=0.35, \beta_2=0.65; t\in(-0.01, 0.12), w\in(-0.01, 0.12)$. The mixture mass consisting of slightly less than 50% solid and slightly more than 50% fluid is fed continuously from the left boundary with zero initial velocities. The solutions are associated with the arc corresponding to t=0.12 on the manifold ν (Fig. 7). The solutions here are quite different from those presented in Fig. 5 for the system (30). The solutions in the variables x and X are quite similar. Also, in the present similarity solutions, even in the final physical variable (X) the solid and fluid fronts are very close to each other. As compared to model (30) and the associated Fig. 5, here both the solid and fluid flow heights drop rapidly in the downstream and tend to reduce negligibly in the far downstream. For very short distance from the position of the flow release, the fluid height dominates slightly, otherwise the solid height dominates. This is accompanied by the flow velocities in which always the fluid velocity dominates over the solid-phase velocity and that both the solid and fluid phase velocities increase rapidly just after the flow release and tend to increase further. In these model solutions, largely the phase velocities and heights tend to depart from one another.

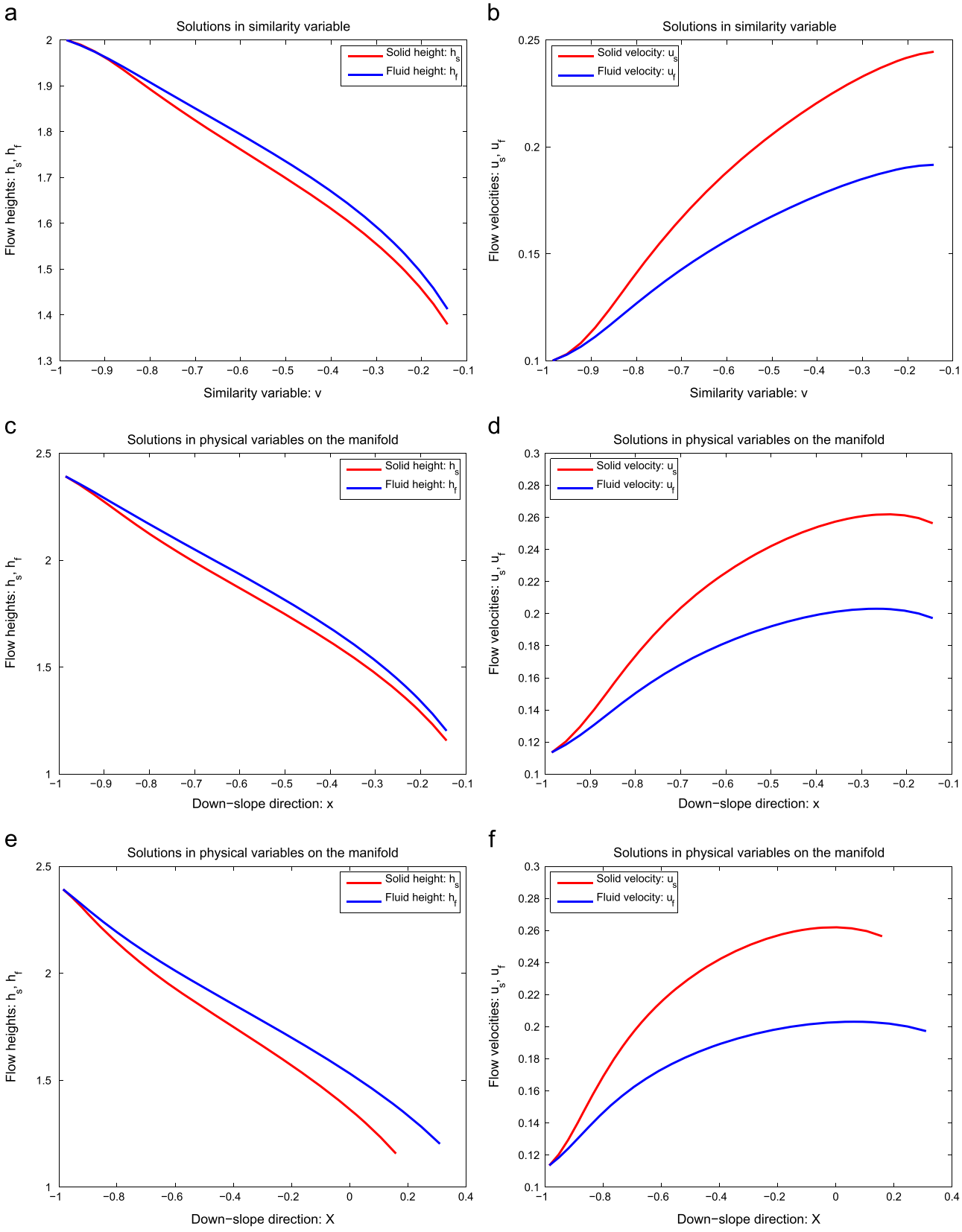

Fig. 4. Solutions to system (30): panels show phase-flow heights and velocities in terms of the similarity variable v (Fig. 3) ((a) and (b)), physical variable x ((c) and (d)), and the physical variable X ((e) and (f)). Solutions reveal strong non-linear and distinct evolutions of the solid and fluid phase dynamics (flow heights and velocities).

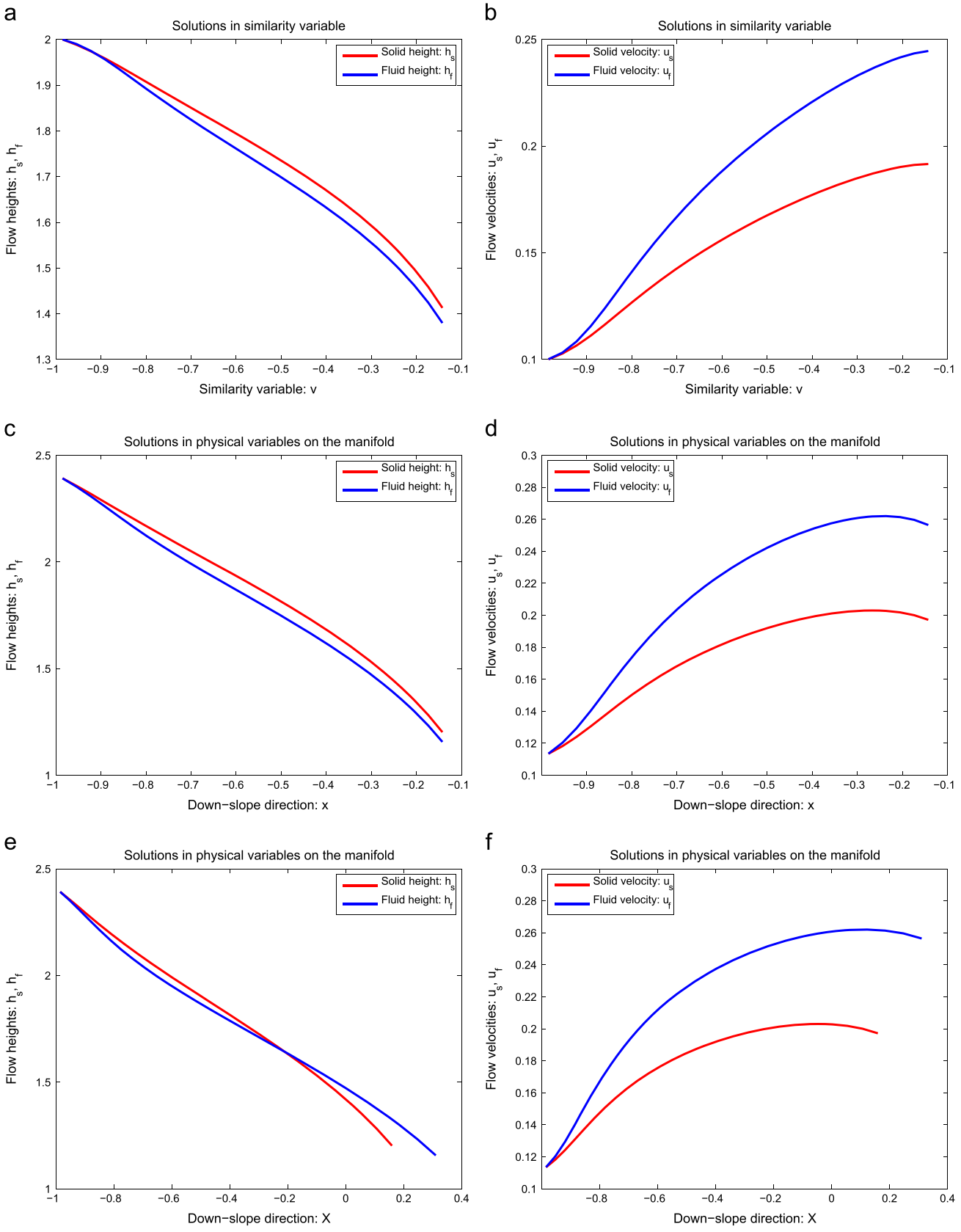

Fig. 5. Solutions to the system (30) with the higher fluid pressure parameter ($\beta_2 > \beta_1$). The panels show the phase-flow heights and velocities in terms of the similarity variable v ((a) and (b)), the physical variable x ((c) and (d)), and the physical variable X ((e) and (f)).

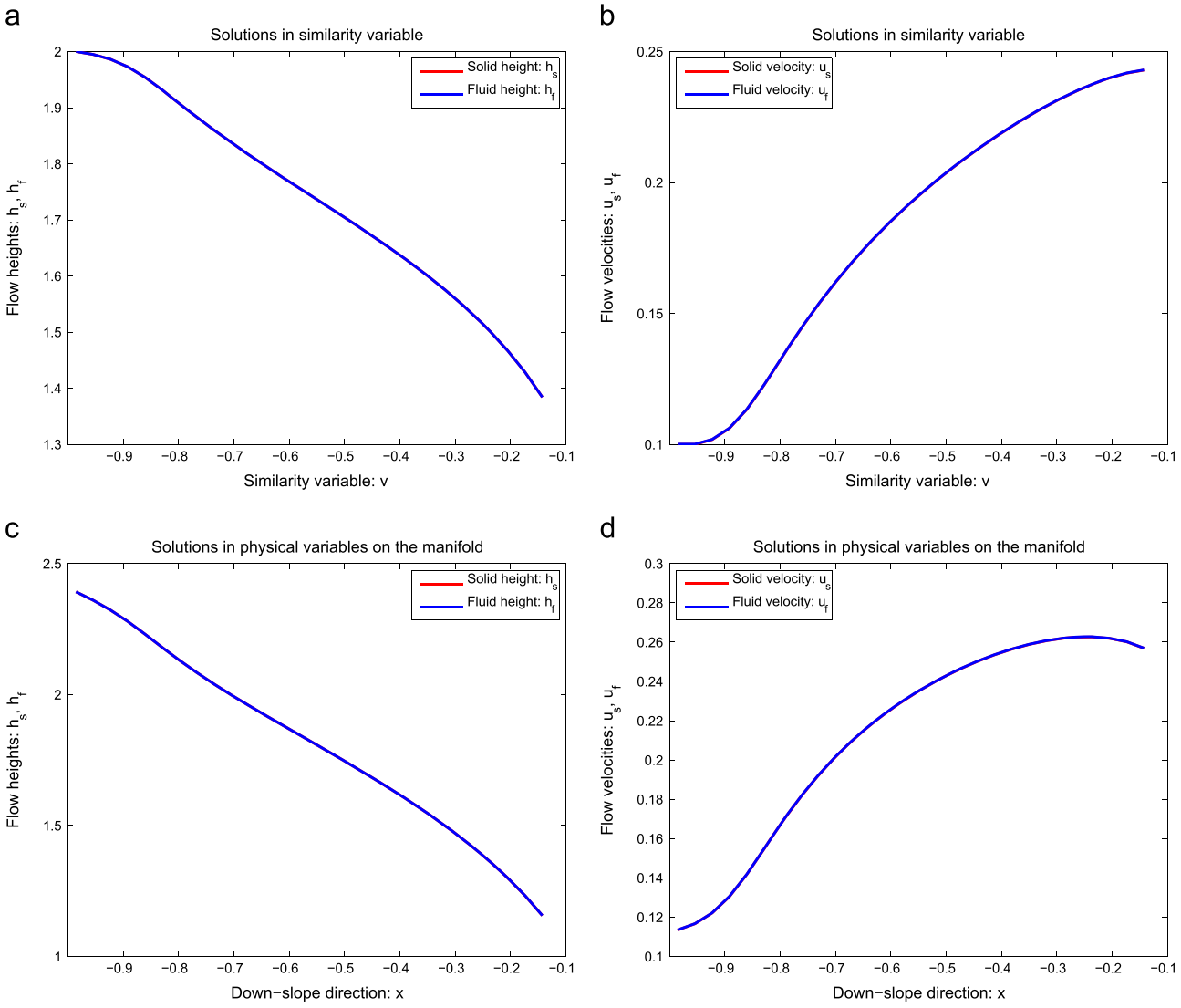

Fig. 6. Solutions to the system (30) with the same pressure parameters $\beta_1 = \beta_2$. The panels reveal that (the phase dynamics) the phase-flow heights and velocities in terms of the similarity variable v (panels (a) and (b)) and the physical variable x (panels (c) and (d)) coincide.

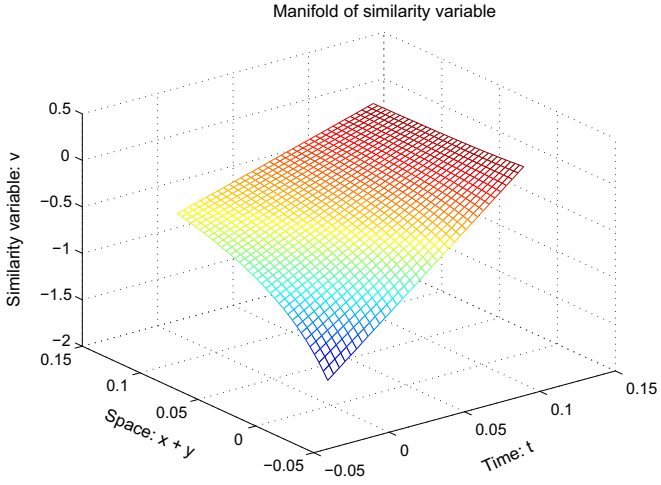

Fig. 7. The manifold v given by (28) for parameter choice: $a_1 = 1.0, a_2 = -1.32; a_3 = 10.50, a_4 = 11.75$.

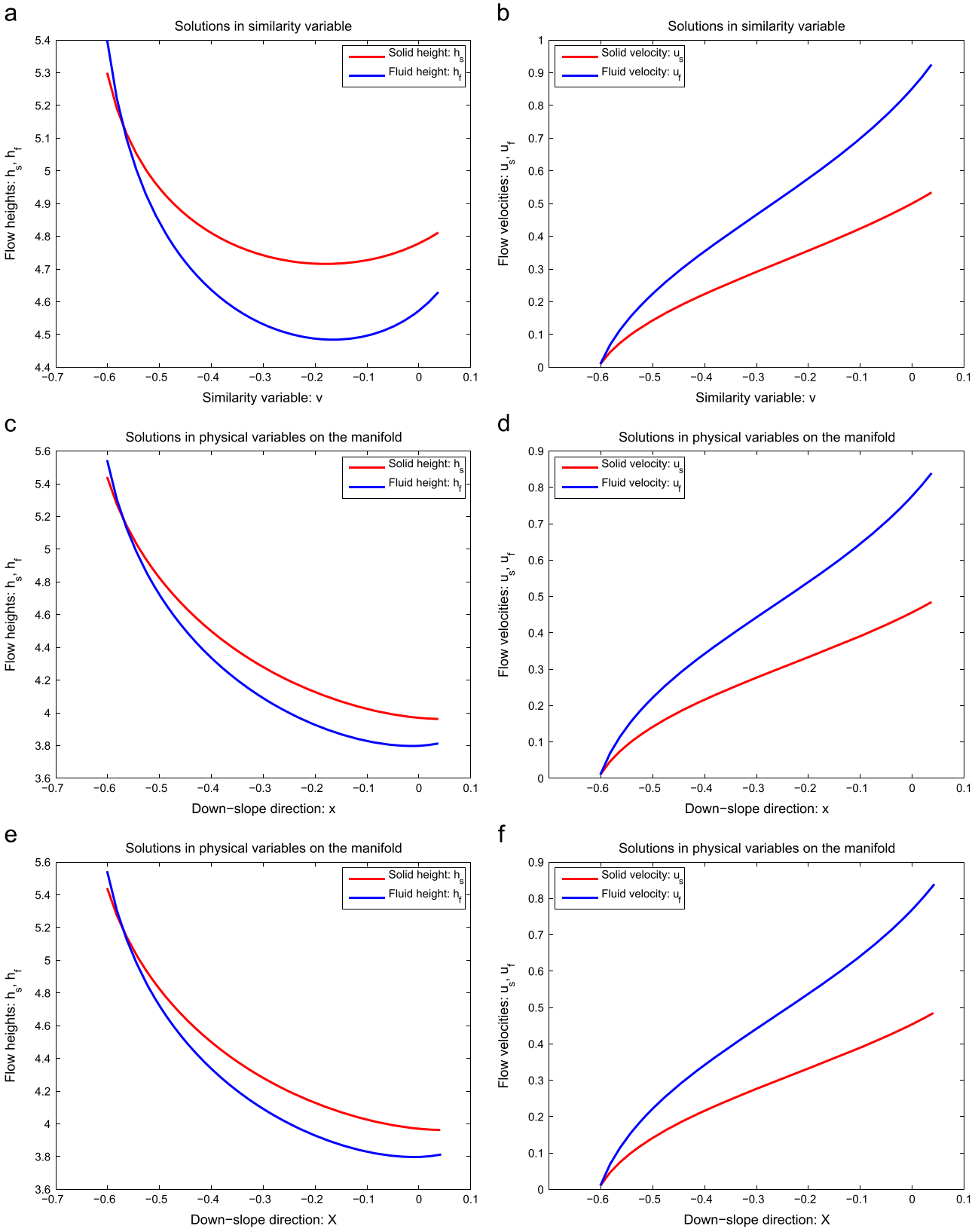

Fig. 8. Solutions to the system (36): panels show phase-flow heights and velocities in terms of the similarity variable v (Fig. 7) ((a) and (b)), physical variable x ((c) and (d)), and the physical variable X ((e) and (f)). These solutions reveal strong non-linear and distinct evolutions of the solid and fluid phase dynamics (flow heights and flow velocities).

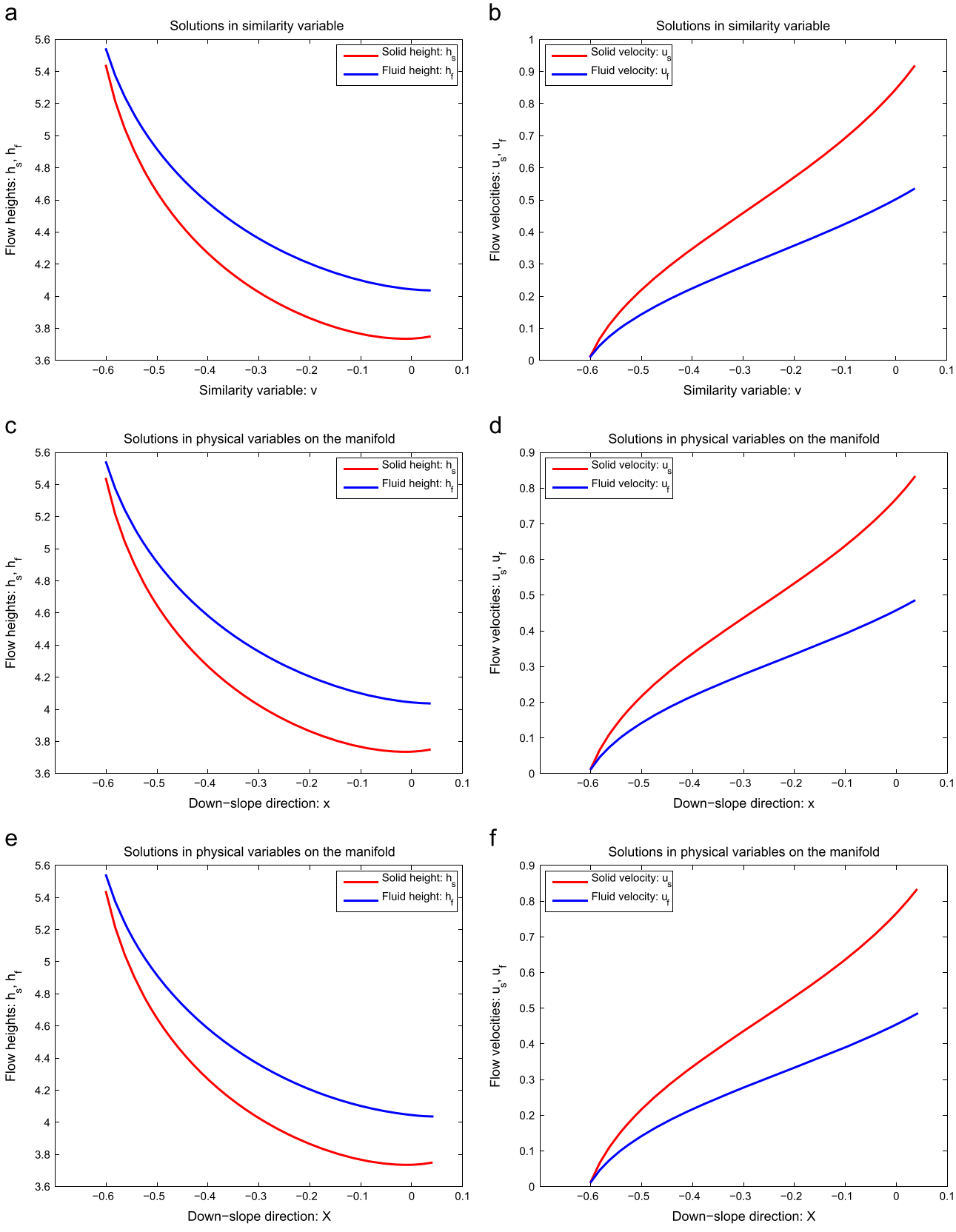

Fig. 9. Solutions to the system (36) with the higher solid pressure parameter ($\beta_1 > \beta_2$). The panels show the phase-flow heights and velocities in terms of the similarity variable ν (panels (a) and (b)), the physical variable x (panels (c) and (d)), and the physical variable X (panels (e) and (f)).

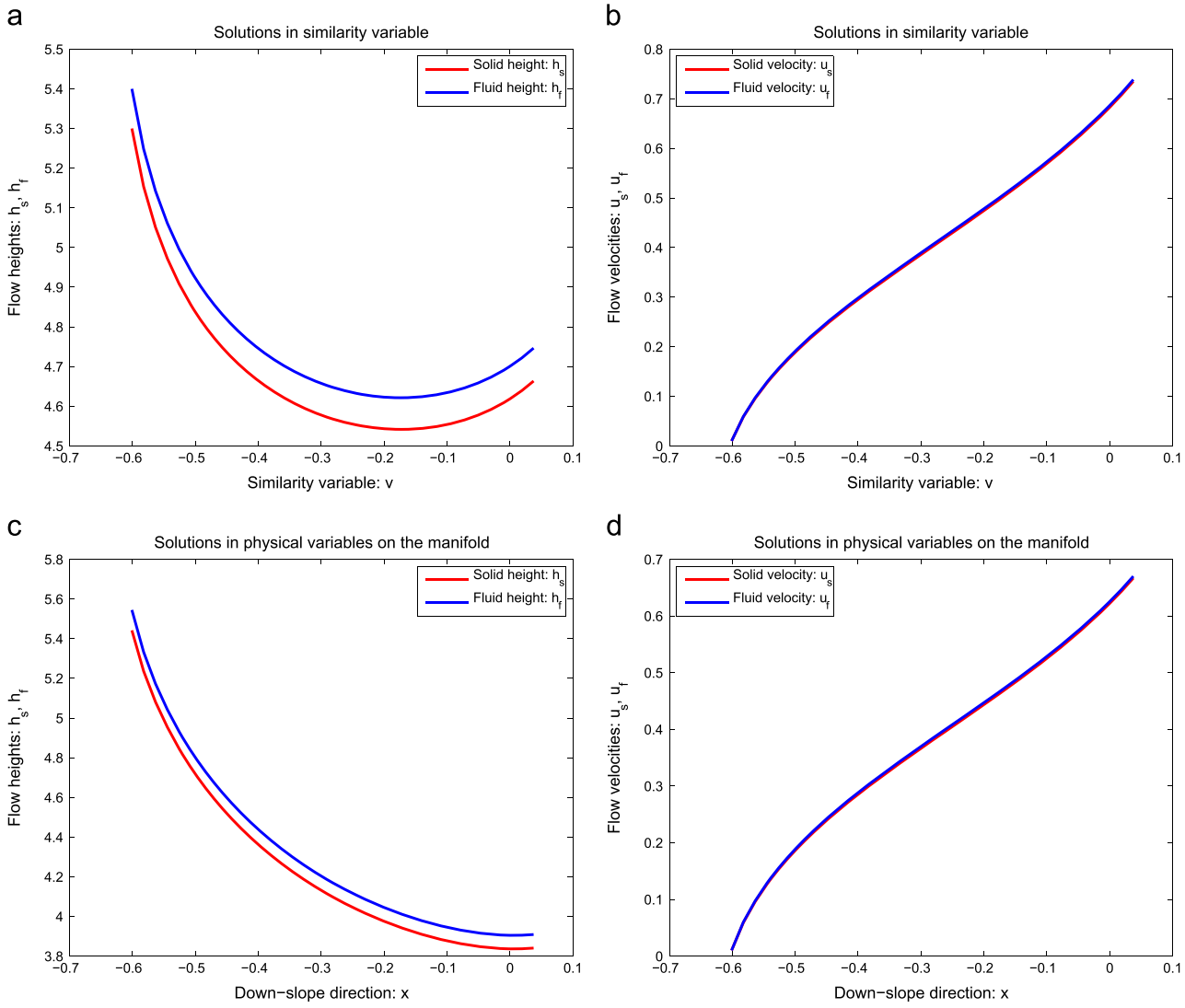

Fig. 10. Solutions to the system (36) with the same pressure parameters. The panels show the phase-flow heights and velocities in terms of the similarity variable v ((a) and (b)), and the physical variable x ((c) and (d)). These solutions reveal that the solid and fluid phase velocities coincide, but not the phase flow depths.

The role of the pressure parameters for the system (36): Next, we analyze the effect of the pressure parameters. For this purpose, we chose the pressure parameters as $\beta_1 = 0.65, \beta_2 = 0.35$ so that the solid pressure dominates. The results are presented in Fig. 9 which show that the dynamics have now been switched, but this switching is different from that in the model (30). The departure of the flow dynamics from one another is more pronounced now than in the previous model (Fig. 4). Next, we consider the solution with the same pressure parameters $\beta_1 = 0.5$ and $\beta_2 = 0.5$. The results as presented in Fig. 10 reveal that only the phase velocities coincide, but the phase flow depths are still different which was not the case with the model (30) for which with the same pressure parameters, both the phase heights and the velocities coincide (Fig. 6) to each other.

7. Reduction to system of ODEs and analysis—non-homogeneous model II

Now we consider the case $a_3 = 0, a_4 \neq 0$ and $a_1 \neq 0$. The similarity variable for this case is

$$v = e^w (a_2 + a_4 t)^{-a_1/a_4}. \tag{37}$$

7.1. Similarity form associated with time element (operator)

Integrating the equations consisting of second and third, second and fourth, second and fifth and second and sixth expressions respectively in (16), we get the similarity forms:

$$\begin{aligned} &\tilde{h}_1(v) = (a_2 + a_4 t)^2 \hat{h}_1(w,t), \quad \tilde{u}_1(v) = (a_2 + a_4 t)\hat{u}_1(w,t); \\ &\tilde{h}_2(v) = (a_2 + a_4 t)^2 \hat{h}_2(w,t), \quad \tilde{u}_2(v) = (a_2 + a_4 t)\hat{u}_2(w,t). \end{aligned} \tag{38}$$

Putting these similarity forms in (14) and (15) we get

$$\begin{bmatrix} -a_1 v + v\tilde{u}_1 & 0 & v\tilde{h}_1 & 0 \\ 0 & -a_1 v + v\tilde{u}_2 & 0 & v\tilde{h}_2 \\ \beta_1 v + 0.5\beta_1 v\tilde{h}_2/\tilde{h}_1 & 0.5\beta_1 v & -a_1 v + v\tilde{u}_1 & 0 \\ 0.5\beta_2 v & \beta_2 v + 0.5\beta_2 v\tilde{h}_1/\tilde{h}_2 & 0 & -a_1 v + v\tilde{u}_2 \end{bmatrix} \begin{bmatrix} d\tilde{h}_1/dv \\ d\tilde{h}_2/dv \\ d\tilde{u}_1/dv \\ d\tilde{u}_2/dv \end{bmatrix} = \begin{bmatrix} 2a_4\tilde{h}_1 \\ 2a_4\tilde{h}_2 \\ a_4\tilde{u}_1 \\ a_4\tilde{u}_2 \end{bmatrix}. \tag{39}$$

7.2. Similarity form associated with spatial element (operator)

We obtain the similarity forms

$$\begin{aligned} &\hat{h}_1(w,t) = \tilde{h}_1(v)e^{-2a_4 w/a_1}, \quad \hat{u}_1(w,t) = \tilde{u}_1(v)e^{-a_4 w/a_1}; \\ &\hat{h}_2(w,t) = \tilde{h}_2(v)e^{-2a_4 w/a_1}, \quad \hat{u}_2(w,t) = \tilde{u}_2(v)e^{-a_4 w/a_1} \end{aligned} \tag{40}$$

by integrating the equations consisting of first and third, first and

Table 1
Lie brackets for the generators $\{V_1, V_2, V_3, V_4, V_5\}$ as in (13) of the Lie algebra $\mathfrak{g}$.

$[,]$	V_1	V_2	V_3	V_4	V_5
V_1	0	0	0	V_1	0
V_2	0	0	0	V_2	0
V_3	0	0	0	0	V_3
V_4	$-V_1$	$-V_2$	0	0	0
V_5	0	0	$-V_3$	0	0

Table 2
The Lie bracket operation for the generators $\{X_1, X_2, X_3, X_4\}$ of the Lie subalgebra $\mathfrak{h}$.

$[,]$	X_1	X_2	X_3	X_4
X_1	0	0	X_1	0
X_2	0	0	0	X_2
X_3	$-X_1$	0	0	0
X_4	0	$-X_2$	0	0

fourth, first and fifth and first and sixth expressions respectively in (16). Substituting these similarity forms into (14) and (15) leads to another system of ODEs:

$$\begin{bmatrix} -a_1v^p+v\tilde{u}_1 & 0 & v\tilde{h}_1 & 0 \\ 0 & -a_1v^p+v\tilde{u}_2 & 0 & v\tilde{h}_2 \\ \beta_1 v+0.5\beta_1 v\tilde{h}_2/\tilde{h}_1 & 0.5\beta_1 v & -a_1v^p+v\tilde{u}_1 & 0 \\ 0.5\beta_2 v & \beta_2 v+0.5\beta_2 v\tilde{h}_1/\tilde{h}_2 & 0 & -a_1v^p+v\tilde{u}_2 \end{bmatrix} \begin{bmatrix} d\tilde{h}_1/dv \\ d\tilde{h}_2/dv \\ d\tilde{u}_1/dv \\ d\tilde{u}_2/dv \end{bmatrix} = \begin{bmatrix} 3a_4\tilde{u}_1\tilde{h}_1/a_1 \\ 3a_4\tilde{u}_2\tilde{h}_2/a_1 \\ a_4(\tilde{u}_1^2+2\beta_1(\tilde{h}_1+\tilde{h}_2))/a_1 \\ a_4(\tilde{u}_2^2+2\beta_2(\tilde{h}_1+\tilde{h}_2))/a_1 \end{bmatrix}. \tag{41}$$

7.3. Further models without time stretching

In the case when $a_2 \neq 0, a_3 \neq 0, a_4 = 0$, the similarity variable is $v = e^t(a_1+a_3w)^{-a_2/a_3}$.

Integrating the equations consisting of second and third, second and fourth, second and fifth and second and sixth expressions respectively in (16), we get the similarity forms:

$$\begin{aligned} &\hat{h}_1(w,t) = \tilde{h}_1(v)e^{2a_3t/a_2}, \quad \hat{u}_1(w,t) = \tilde{u}_1(v)e^{a_3t/a_2}; \\ &\hat{h}_2(w,t) = \tilde{h}_2(v)e^{2a_3t/a_2}, \quad \hat{u}_2(w,t) = \tilde{u}_2(v)e^{a_3t/a_2}. \end{aligned} \tag{42}$$

Substituting the similarity forms (42) into (14) and (15), we get a further new system of ODEs:

$$\begin{bmatrix} v-a_2v^q\tilde{u}_1 & 0 & -a_2v^q\tilde{h}_1 & 0 \\ 0 & v-a_2v^q\tilde{u}_2 & 0 & -a_2v^q\tilde{h}_2 \\ -\beta_1a_2v^q-0.5\beta_1a_2v^q\tilde{h}_2/\tilde{h}_1 & -0.5\beta_1a_2v^q & v-a_2v^q\tilde{u}_1 & 0 \\ -0.5\beta_2a_2v^q & -\beta_2a_2v^q-0.5\beta_2a_2v^q\tilde{h}_1/\tilde{h}_2 & 0 & v-a_2v^q\tilde{u}_2 \end{bmatrix} \begin{bmatrix} d\tilde{h}_1/dv \\ d\tilde{h}_2/dv \\ d\tilde{u}_1/dv \\ d\tilde{u}_2/dv \end{bmatrix} = \begin{bmatrix} -2a_3\tilde{h}_1/a_2 \\ -2a_3\tilde{h}_2/a_2 \\ -a_3\tilde{u}_1/a_2 \\ -a_3\tilde{u}_2/a_2 \end{bmatrix}. \tag{43}$$

Again, integrating the equations consisting of first and third, first and fourth, first and fifth and first and sixth expressions respectively in (16) we get the similarity forms:

$$\begin{aligned} &\hat{h}_1(w,t) = (a_1+a_3w)^2\tilde{h}_1(v), \quad \hat{u}_1(w,t) = (a_1+a_3w)\tilde{u}_1(v); \\ &\hat{h}_2(w,t) = (a_1+a_3w)^2\tilde{h}_2(v), \quad \hat{u}_2(w,t) = (a_1+a_3w)\tilde{u}_2(v). \end{aligned} \tag{44}$$

Substituting the similarity forms (44) into (14) and (15) gives yet another new system:

$$\begin{bmatrix} 1-a_2\tilde{u}_1 & 0 & -a_2\tilde{h}_1 & 0 \\ 0 & 1-a_2\tilde{u}_2 & 0 & -a_2\tilde{h}_2 \\ -\beta_1a_2-0.5\beta_1a_2\tilde{h}_2/\tilde{h}_1 & -0.5\beta_1a_2 & 1-a_2\tilde{u}_1 & 0 \\ -0.5\beta_2a_2 & -\beta_2a_2-0.5\beta_2a_2\tilde{h}_1/\tilde{h}_2 & 0 & 1-a_2\tilde{u}_2 \end{bmatrix} \begin{bmatrix} d\tilde{h}_1/dv \\ d\tilde{h}_2/dv \\ d\tilde{u}_1/dv \\ d\tilde{u}_2/dv \end{bmatrix} = \begin{bmatrix} 0 \\ 0 \\ 0 \\ 0 \end{bmatrix}. \tag{45}$$

Since the systems (39), (41), (43) and (45) are supposed to produce similar solutions as produced by the systems (30) and (36), here we do not discuss the results of these systems.

8. Summary

We present some new Lie theoretic analytical solutions to a system of partial differential equations describing a two-phase debris mass flow as a mixture of solid particles and fluid down a slope. New analytical models and results demonstrate that there are strong phase-interactions. Most of the solutions presented here are extensions to the previously obtained solutions for single-phase granular, debris and hydraulic channel flows.

We systematically studied the phase interactions between the solid and fluid components. This is achieved by constructing model solutions by employing the Lie group symmetry methods. For this, we considered a two-phase mass flow model [1] that includes, as driving forces, the gravity, friction, buoyancy, phase-interactions and hydraulic pressure gradients for the solid and fluid phases. There are strong non-linear interactions between the phases via these forces and volume fractions. These forces are mechanically important in explaining the physics of the two-phase gravity mass flows. Such flows are not considered in the previous models as done here for the mixture flows in connection to the application of Lie group. These non-linear phase-interactions pose great challenges in constructing exact solutions as compared to the effective single-phase gravity mass flows. So, our mixture mass flow model is different from the existing models and the problem we are considering here is fundamentally novel.

With the Lie group symmetry methods, we reduced the system of PDEs to systems of ODEs which may be solvable analytically. We show, with the Lie symmetry transformations, the similarity variable for the considered two-phase mass flow takes a form of a product of two exponents for time and space and that the similarity form is expressed as a product of an exponent function and the original dynamical variables. Our subalgebras generalize several previously considered subalgebras for gravity mass flows as the new subalgebras are associated with the two-phase gravity mass flows. New solutions largely generalize most of the similarity variables and forms obtained previously by the same methods. We show that the choice of the group parameters determines the similarity variables, similarity forms and finally different reduced models, dynamics of the reduced systems and symmetry preserving solutions. For some choices of group parameters, the reduced systems become homogeneous set of ODEs. Particularly, the non-stretching of the time and space generates homogeneous ODEs for the similarity forms implicitly in similarity variables, that have been solved analytically to yield exact solutions. For given sets of general group parameters, the similarity reduced forms result in different system of non-homogeneous ODEs for which similarity solutions are presented numerically.

For the homogeneous model, the solutions reveal strong solid–fluid phase interactions, and non-linear relationships between the flow dynamical variables (the solid- and fluid-heights and solid- and fluid-phase velocities). After the mass release from the top of the slope, both the solid and the fluid masses rarefy resulting in the decrease of the solid and the fluid heights along the down-slope direction. As the mass accelerates, the corresponding solid-

and fluid-phase velocities increase. Several important relationships between the flow heights and velocities are revealed. Although, the flow velocities vary quadratically with the corresponding phase-flow heights, solid phase-velocity varies concavely with the solid phase height, whereas this relationship is convex for fluid phase. Similarly, the solid and fluid heights, and the solid and fluid phase velocities vary strongly non-linearly. At a given downslope position, we observe that the flow velocity increases quadratically as a function of the flow height. Interestingly, as the solid velocity increases the fluid velocity also increases quadratically. Importantly, although the boundary conditions for the solid and fluid heights and solid and fluid velocities are the same, they evolve fundamentally differently. As the flow cascades down slope, the solid-phase flow depth decreases faster than the fluid-phase flow depth. This resulted in the higher flow velocity of the solid-phase as compared to the fluid-phase velocity. Both the solid and the fluid phase velocities are increasing rapidly as the flow is released, then tend to slow down.

The results for the non-homogeneous models are more complex as they could include more physics of the flow. Evolutions of the phase-heights and phase-velocities are discussed for different non-homogeneous models. The solutions as presented for the similarity and physical variables, in general, show fundamentally different behavior. As the flow is released, due to shearing, the flow depths for both the solid and the fluid decrease, whereas the phase-velocities increase. Nevertheless, the rate of decrease in phase-heights and increase in phase-velocities and their local dominance depends on the choice of reduced model and physical parameters. Depending on this, the drop in solid and fluid heights may be rapid or slow, concave or convex and may tend to deform negligibly or strongly in the far down stream. Similarly, the flow velocities may increase rapidly just after the flow release and tend to attain steadiness or continue to increase. The solutions for the phase velocities and heights may depart from one another or come a bit closer as the flow propagates down slope.

We analyzed in detail the effect of different physical parameters. We observed that by switching the pressure parameters (from solid to fluid and vice versa) the results are also just switched. To test the model and solution performances, we set the same solid and fluid pressure parameters. Interestingly, for one model, the solutions for the solid and fluid flow heights and flow velocities coincide, whereas for another model, only the phase-flow velocities coincide, but the phase-flow depths differ. Further, physically relevant and particularly important aspects are that: whether the solid or the fluid heights and velocities and whether the fluid- or the solid-phase front dominates along the slope depends, including others, on the choice of the pressure parameters and frictions. Nevertheless, the dominance of the solid or the fluid velocity results mainly from the pressure parameter and the front position dominance by fluid (or solid) is determined by the net driving force.

These solutions reveal strong non-linear and distinct evolutions of the solid and fluid phase dynamics of two-phase mass flows (flow heights and flow velocities). These results show that phase-interactions are important and that our solutions derived with the Lie algebra symmetry produce physically relevant, compatible and consistent results and observable phenomena of two-phase flows in nature. The results highlight the basic physics associated with the two-phase nature of the mixture flow. Such simultaneous and explicit solutions, as constructed by employing the Lie algebra, for the phase-heights and phase-velocities for the solid and fluid as a two-phase mixture material moves down-slope is novel and not yet available in the literature.

Acknowledgments

We thank the reviewer for constructive feedback that helped to improve the manuscript significantly. Santosh Kandel would like to thank Max Planck Institute for Mathematics where a part of this work was carried out. Shiva P. Pudasaini acknowledges the financial support provided by the German Research Foundation (DFG) through the research project, PU 386/3-1: “Development of a GIS-based Open Source Simulation Tool for Modelling General Avalanche and Debris Flows over Natural Topography” within a transnational research project, D-A-CH.

References

[1] S.P. Pudasaini, A general two-phase debris flow model, J. Geophys. Res. 117 (2012) F03010 28 pp.
[2] J.S. O'Brien, P.J. Julien, W.T. Fullerton, Two-dimensional water flood and mudflow simulation, J. Hydraul. Eng. 119 (2) (1993) 244–261.
[3] O. Hungr, A model for the runout analysis of rapid flow slides, debris flows, and avalanches, Can. Geotech. J. 32 (1995) 610–623.
[4] R.M. Iverson, R.P. Denlinger, Flow of variably fluidized granular masses across three-dimensional terrain: 1. Coulomb mixture theory, J. Geophys. Res. 106 (B1) (2001) 537–552.
[5] E.B. Pitman, L. Le, A two-fluid model for avalanche and debris flows, Philos. Trans. R. Soc. A 363 (2005) 1573–1602.
[6] S.P. Pudasaini, Y. Wang, K. Hutter, Modelling debris flows down general channels, Nat. Hazards Earth Syst. Sci. 5 (2005) 799–819.
[7] T. Takahashi, Debris Flow: Mechanics Prediction and Countermeasures, Taylor and Francis, New York, 2007.
[8] K. Hutter, L. Schneider, Important aspects in the formulation of solid–fluid debris-flow models. Part I. Thermodynamic implications, Contin. Mech. Thermodyn. 22 (2010) 363–390.
[9] K. Hutter, L. Schneider, Important aspects in the formulation of solid–fluid debris-flow models. Part II. Constitutive modelling, Contin. Mech. Thermodyn. 22 (2010) 391–411.
[10] S.P. Pudasaini, Some exact solutions for debris and avalanche flows, Phys. Fluids 23 (4) (2011) 043301 16 pp.
[11] D. Sahin, N. Antar, T. Ozer, Lie group analysis of gravity currents, Nonlinear Anal. Real World Appl. 11 (2) (2010) 978–994.
[12] S.P. Pudasaini, M. Krautblatter, A two-phase mechanical model for rock-ice avalanches, J. Geophys. Res. Earth Surf. 119 (2014) 2272–2290.
[13] B.W. McArdell, P. Bartelt, J. Kowalski, Field observations of basal forces and fluid pore pressure in a debris flow, Geophys. Res. Lett. 34 (2007) L07406 4 pp.
[14] D. Schneider, C. Huggel, W. Haeberli, R. Kaitna, Unraveling driving factors for large rock–ice avalanche mobility, Earth Surf. Process. Landforms 36 (14) (2011) 1948–1966.
[15] D. Schneider, P. Bartelt, J. Caplan-Auerbach, M. Christen, C. Huggel, B. W. McArdell, Insights into rock–ice avalanche dynamics by combined analysis of seismic recordings and a numerical avalanche model, J. Geophys. Res. 115 (2010) F04026 20 pp.
[16] R. Sosio, G.B. Crosta, J.H. Chen, O. Hungr, Modelling rock avalanche propagation onto glaciers, Quat. Sci. Rev. 47 (2012) 23–40.
[17] S.P. Pudasaini, Dynamics of submarine debris flow and tsunami, Acta Mech. 225 (2014) 2423–2434.
[18] S. Lie, Theorie der transformations Gruppen, I. Math. Ann. 16 (1880) 441–528.
[19] L.V. Ovsiannikov, Group Analysis of Differential Equations, Academic Press, Inc., New York-London, 1982.
[20] B.A. Kupershmidt, Y.I. Manin, Long-wave equation with free boundary I: conservation laws and solutions, Funct. Anal. Appl. 3 (11) (1977) 188–197.
[21] D. Roberts, The general Lie group and similarity solutions for the one dimensional Vlasov–Maxwell equations, J. Plasma Phys. 33 (1985) 219.
[22] S.V. Meleshko, Group properties of equations of motions of a viscoelastic medium, Model. Mekh. 2 (19) (1988) 114–126.
[23] G. Bluman, S. Kumei, Symmetries and Differential Equations, Springer-Verlag, Berlin, 1989.
[24] V.F. Kovalev, S.V. Krivenko, V. Pustovalov, Lie symmetry and group for the boundary value problem, Differ. Uravn. 10 (1994) 30.
[25] T. Özer, On symmetry group properties and general similarity forms of the Benney equations in the Lagrangian variables, J. Comput. Appl. Math. 169 (2004) 297–313.
[26] T. Özer, Symmetry group analysis of Benney system and application for the shallow-water equation, Mech. Res. Comm. 32 (2005) 241–254.
[27] T. Özer, N. Antar, The similarity forms and invariant solutions of two-layer shallow-water equations, Nonlinear Anal.: Real World Appl. 9 (2008) 791–810.
[28] P.J. Olver, Applications of Lie Groups to Differential Equations, 2nd ed., Graduate Texts in Mathematics, vol. 107, Springer-Verlag, New York, 1993.
[29] R.L. Anderson, V.A. Baikov, R.K. Gazizov, W. Hereman, N.H. Ibragimov, F. M. Mahomed, S.V. Meleshko, M.C. Nucci, P.J. Olver, M.B. Sheftel', A.V. Turbiner, E.M. Vorob'ev, CRC Handbook of Lie Group Analysis of Differential Equations, vol. 3, CRC Press, Boca Raton, FL, 1996.

[30] N.H. Ibragimov, A.V. Aksenov, V.A. Baikov, V.A. Chugunov, R.K. Gazizov, A.G. Meshkov, in: N.H. Ibragimov (Ed.), CRC Handbook of Lie Group Analysis of Differential Equations, Applications in Engineering and Physical Sciences, vol. 2, CRC Press, Boca Raton, FL, 1995.
[31] W.F. Ames, R.L. Anderson, V.A. Dorodnitsyn, E.V. Ferapontov, R.K. Gazizov, N. H. Ibragimov, S.R. Svirshchevskiĭ, CRC Handbook of Lie Group Analysis of Differential Equations, vol. 1, CRC Press, Boca Raton, FL, 1994.
[32] P.E. Hydon, Symmetry Methods for Differential Equations, Cambridge Texts in Applied Mathematics, Cambridge University Press, Cambridge, 2000.
[33] J.W. Rottman, R.E. Grundy, The approach to self-similarity of the solutions of the shallow-water equations representing gravity current releases, J. Fluid. Mech. 156 (1985) 39–53.
[34] P. Glaister, Similarity solutions of the shallow-water equations, J. Hydraul. Res. 29 (1991) 107–116.
[35] J. Gratton, C. Vigo, Self-similarity gravity currents with variable inflow revisited: Plane currents, J. Fluid. Mech. 258 (1994) 77–104.
[36] R.T. Sekhar, V.D. Sharma, Similarity analysis of modified shallow water equations and evolution of weak waves, Commun. Nonlinear Sci. Numer. Simul. 17 (2012) 630–636.
[37] S. Szatmari, A. Bihlo, Symmetry analysis of a system of modified shallow-water equations, Commun. Nonlinear Sci. Numer. Simul. 19 (3) (2014) 530–537.
[38] V. Chugunov, J.M.N.T. Gray, K. Hutter, Group Theoretic Methods and Similarity Solutions of the Savage-Hutter Equations, Springer, Berlin, 2003.
[39] N. Zahibo, E. Pelinovsky, T. Talipova, I. Nikolkina, Savage-Hutter model for avalanche dynamics in inclined channels: analytical solutions, J. Geophys. Res. 115 (2010) B03402 18 pp.
[40] S.P. Pudasaini, K. Hutter, S.S. Hsiau, S.C. Tai, Y. Wang, R. Katzenbach, Rapid flow of dry granular materials down inclined chutes impinging on rigid walls, Phys. Fluids 19 (5) (2007) 053302 17 pp.